Journal of Human Genetics (2013) 58, 711–719

www.nature.com/jhg

ORIGINAL ARTICLE

YY1 binds to *α-synuclein* 3′-flanking region SNP and stimulates antisense noncoding RNA expression

Ikuko Mizuta[1,2], Kazuaki Takafuji[3], Yuko Ando[1], Wataru Satake[1], Motoi Kanagawa[1], Kazuhiro Kobayashi[1], Shushi Nagamori[3], Takayuki Shinohara[1], Chiyomi Ito[1], Mitsutoshi Yamamoto[4], Nobutaka Hattori[5], Miho Murata[6], Yoshikatsu Kanai[3], Shigeo Murayama[7], Masanori Nakagawa[8] and Tatsushi Toda[1]

***α-synuclein* (*SNCA*) is an established susceptibility gene for Parkinson's disease (PD), one of the most common human neurodegenerative disorders. Increased SNCA is considered to lead to PD and dementia with Lewy bodies. Four single-nucleotide polymorphisms (SNPs) in *SNCA* 3′ region were prominently associated with PD among different ethnic groups. To examine how these SNPs influence disease susceptibility, we analyzed their potential effects on *SNCA* gene expression. We found that rs356219 showed allele-specific features. Gel shift assay using nuclear extracts from SH-SY5Y cells showed binding of one or more proteins to the protective allele, rs356219-A. We purified the rs356219-A–protein complex with DNA affinity beads and identified a bound protein using mass spectrometry. This protein, YY1 (Yin Yang 1), is an ubiquitous transcription factor with multiple functions. We next investigated *SNCA* expression change in SH-SY5Y cells by YY1 transfection. We also analyzed the expression of antisense noncoding RNA (ncRNA) *RP11-115D19.1* in *SNCA* 3′-flanking region, because rs356219 is located in intron of *RP11-115D19.1*. Little change was observed in *SNCA* expression levels; however, *RP11-115D19.1* expression was prominently stimulated by YY1. In autopsied cortices, positive correlation was observed among *RP11-115D19.1*, *SNCA* and *YY1* expression levels, suggesting their functional interactions *in vivo*. Knockdown of *RP11-115D19.1* increased *SNCA* expression significantly in SH-SY5Y cells, suggesting its repressive effect on *SNCA* expression. Our findings of the protective allele-specific YY1 and antisense ncRNA raised a novel possible mechanism to regulate *SNCA* expression.**
Journal of Human Genetics (2013) **58,** 711–719; doi:10.1038/jhg.2013.90; published online 12 September 2013

Keywords: α-*synuclein*; association; ncRNA; Parkinson's disease susceptibility; SNP; YY1

INTRODUCTION

Parkinson's disease (PD) (OMIM 168600) is one of the most common human neurodegenerative disorders, affecting 1–2% of people aged ⩾65 years.[1] Clinical features of PD (parkinsonism) include resting tremor, bradykinesia, rigidity and postural instability. PD is characterized pathologically by the loss of dopaminergic neurons in the substantia nigra of the midbrain and by the presence of intracellular inclusions known as Lewy bodies.[2]

Linkage studies for Mendelian-inherited PD have identified autosomal dominant genes, including *α-synuclein* (*SNCA*) and *LRRK2*, as well as the autosomal recessive genes *parkin*, *PINK1*, *DJ-1*, *ATP13A2*, *PLA2G6* and *FBXO7*.[3,4] However, Mendelian-inherited PD is rare compared with the far more common sporadic PD, a complex disorder caused by multiple genetic and environmental factors.[5]

SNCA was the first-identified causal gene for Mendelian-inherited PD.[6] The missense mutation A53T was identified in the original autosomal-dominant family, followed by confirmation of SNCA protein as a major component of Lewy bodies, the pathological hallmark of PD in both Mendelian-inherited and sporadic cases.[6,7] To date, three missense mutations and multiplication of *SNCA* have been identified in familial PD. Missense mutations are thought to increase the aggregation of SNCA protein. In patients with triplication of the *SNCA* locus, a doubling of wild-type *SNCA* gene dosage by triplication has been shown to result in the doubling of mRNA and protein expression in blood and in the brain.[8,9] Duplication of *SNCA* has also been implicated in familial PD. Patients with *SNCA* duplications show much milder clinical features than do those with *SNCA* triplications, more closely resembling sporadic cases.[10,11]

SNCA is also a causal gene for Mendelian-inherited dementia with Lewy bodies (DLB) (OMIM 127750). DLB, usually sporadic, is characterized clinically by dementia and parkinsonism and

[1]Division of Neurology/Molecular Brain Science, Kobe University Graduate School of Medicine, Kobe, Japan; [2]Department of Neurology, Graduate School of Medical Science, Kyoto Prefectural University of Medicine, Kyoto, Japan; [3]Division of Bio-system Pharmacology, Department of Pharmacology, Graduate School of Medicine, Osaka University, Suita, Japan; [4]Department of Neurology, Kagawa Prefectural Central Hospital, Takamatsu, Japan; [5]Department of Neurology, Juntendo University School of Medicine, Tokyo, Japan; [6]Department of Neurology, National Center Hospital, National Center of Neurology and Psychiatry, Kodaira, Japan; [7]Department of Neuropathology, Tokyo Metropolitan Institute of Gerontology, Tokyo, Japan and [8]North Medical Center, Kyoto Prefectural University of Medicine, Kyoto, Japan
Correspondence: Professor T Toda, Division of Neurology/Molecular Brain Science, Kobe University Graduate School of Medicine, 7-5-1 Kusunoki-chou, Chuo-ku, Kobe 650-0017, Japan.
E-mail: toda@med.kobe-u.ac.jp
Received 24 April 2013; revised 31 July 2013; accepted 2 August 2013; published online 12 September 2013

pathologically by widespread Lewy bodies. According to the overlapped features, PD and DLB are collectively called Lewy body diseases (LBD).

A popular hypothesis is that SNCA aggregation has a crucial role in neuronal loss and Lewy body formation and that increased SNCA leads to LBD. In this scenario, PD-associated *SNCA* polymorphisms might influence *SNCA* expression levels in sporadic PD. We and the others have previously reported that single-nucleotide polymorphisms (SNPs) in the *SNCA* 3′region were prominently associated with sporadic PD in both the Japanese and European populations.[12,13] Moreover, our recent genome-wide association study (GWAS) in the Japanese population,[14] as well as a GWAS analysis in individuals of European ancestry,[15] confirmed a strong association with the *SNCA* 3′region. In this report, we have examined how *SNCA* SNPs might influence LBD susceptibility.

MATERIALS AND METHODS

Genotyping

As described previously,[13] we recruited 882 unrelated sporadic PD patients (age: 64.9 ± 9.8 years; male/female ratio: 0.79) and 938 unrelated controls (age: 45.3 ± 16.3 years; male/female ratio: 1.10). The diagnosis of idiopathic PD was based on the presence of ⩾2 of the cardinal features of PD (tremor, rigidity, bradykinesia and postural instability), according to the criteria for sporadic PD.[16] Patients were evaluated by certified neurologists specializing in PD. The average age of onset was 57.4 ± 10.9 years. Forty-two patients showed early onset of PD (< 40 years of age), and 51 patients had a positive family history of PD. Patients who carried *parkin* mutations were excluded. All patients and controls were of Japanese ancestry. Informed consent was obtained from each individual, and approval for the study was obtained from the University Ethical Committees. Genomic DNA was extracted from the whole blood using FlexGene (Qiagen GmbH, Hilden, Germany). The rs356219, rs356220 and rs356203 SNPs were genotyped using TaqMan (Applied Biosystems, Lifetechnologies Corp., Carlsbad, CA, USA). SNPAlyze software (DYNACOM, Chiba, Japan) was used for pairwise linkage disequilibrium analysis (Lewontin's coefficient, D′, and standardized coefficient, *r*).

Luciferase assay

DNA fragments of ~250 bp corresponding to the regions containing four *SNCA* SNPs (rs356219, rs356220, rs356165 and rs356203) were amplified by PCR using heterozygous genomic DNA as template and then cloned into the SalI site of the pGL3-promoter vector (Promega Corporation, Madison, WI, USA). The orientation and allele identity of the insert were determined by DNA sequence analysis. Primer sequences used for PCR are listed in Supplementary Table 1. The human neuroblastoma cell line SH-SY5Y was grown in Dulbecco's Modified Eagle's medium supplemented with 10% fetal bovine serum and antibiotics. We transfected cells (3×10^5 cells per well on 24-well plates) with 360 ng of each construct and 40 ng of pRL-TK vector (Promega), as an internal control for transfection efficiency, using Effectene (Qiagen). After 48 h, cells were solubilized, and luciferase activity was measured using the dual luciferase assay system (Promega).

Preparation of nuclear extract

Nuclear extracts from SH-SY5Y cells were prepared as previously described, with minor modifications.[17] In brief, cells were washed and re-suspended in buffer A (10 mM 4-(2-hydroxyethyl)-1-piperazineethanesulfonic acid (HEPES)-KOH pH7.8, 10 mM KCl, 0.1 mM EDTA pH8.0, 0.1% NP-40, 1 mM dithiothreitol (DTT) and protease inhibitor cocktail (NACALAI TESQUE, Inc., Kyoto, Japan)). Nuclei were pelleted and re-suspended in buffer C (50 mM HEPES-KOH pH7.8, 420 mM KCl, 0.1 mM EDTA pH8.0, 5 mM $MgCl_2$, 2% glycerol, 1 mM DTT and protease inhibitor cocktail). After vortexing every 5 min for 30 min on ice, the samples were centrifuged, and the supernatants were used as nuclear extract.

Gel shift assay

Gel shift assays were performed as previously described.[18] SH-SY5Y nuclear extract (5–10 μg protein) was incubated with 0.031 pmol of 33-bp oligonucleotides (Supplementary Table 2) labeled with digoxigenin-11-ddUTP in 20 μl of binding buffer (20 mM HEPES pH7.6, 1 mM EDTA, 10 mM $(NH_4)_2SO_4$, 1 mM DTT, 0.2% Tween 20 and 30 mM KCl) containing 1 μg of poly(dI-dC) for 20 min, using the DIG gel shift kit (Roche Diagnostics, Mannheim, Germany). For competition studies, nuclear extract was pre-incubated with 3.85 pmol of unlabeled oligonucleotide before addition of the labeled probe. Supershift assays were performed by incubating the protein–DNA complexes with 0.8 μg of rabbit immunoglobulin G or rabbit polyclonal anti-YY1 (anti-Yin Yang 1; Active Motif, Carlsbad, CA, USA) for 5 min. The protein–DNA complexes were separated on DNA retardation polyacrylamide gels (Invitrogen, Lifetechnologies Corp., Carlsbad, CA, USA) and transferred to Hybond-N+ Nylon membrane (GE Healthcare, Amersham Place, UK). All assays and gel electrophoresis procedures were performed at 4 °C. Signal detection was performed using the CSPD chemiluminescent detection system (Roche Diagnostics).

Ultraviolet (UV) cross-linking

The size of the rs356219-A binding protein was determined by UV cross-linking. We incubated 0.05 pmol of ^{32}P-labeled 33 bp rs356219-A oligonucleotide with SH-SY5Y nuclear extract and 6.16 pmol of unlabeled 33 bp competitor (rs356219-G or -A) for 15 min at 4 °C in the solution used for the gel shift assays. DNA–protein complexes were transferred to a flat-bottom 96-well plate, placed on a transilluminator and irradiated (312 nm, 15 min at 4 °C). Samples were run on 10% NuPAGE Novex Bis-Tris gels (Invitrogen), dried and autoradiographed.

Purification of the rs356219-A binding protein using affinity magnetic beads

Oligonucleotides containing rs356219-A with 5′-TCGA-3′ linkers were ligated in a head-to-tail manner and inserted into the SalI site of the pGL3-promoter vector (Promega). A fragment with 14 tandem repeats of rs356219-A was amplified from the plasmid by PCR using a biotin-labeled forward primer (5′-GGTAAAATCGATAAGGATCC-3′) and a non-labeled reverse primer (5′-TTGAAGGCTCTCAAGGGCAT-3′). The biotinylated PCR product (30 pmol) was bound to 1 mg of Dynabeads M-280 streptavidin (Dynal, Life Technologies, Carlsbad, CA, USA). Fifty microliters of SH-SY5Y nuclear extract, prepared with Buffer C containing 200 mM KCl, was precleared in 1 ml of binding buffer in the presence of 1 mg of unbound beads and 144 pmol of 33 bp non-labeled competitor rs356219-A or -G. Following magnetic separation, the supernatant was incubated with 1 mg of probe-bound Dynabeads for 30 min at 4°C. The beads were washed five times and then eluted sequentially, twice with 40 μl elution buffer (20 mM HEPES-KOH pH7.6, 1 mM EDTA, 10 mM $(NH_4)_2SO_4$, 1 mM DTT, 0.2% Tween 20, protease inhibitor cocktail and 10% glycerol) containing 200 mM KCl and twice with 40 μl elution buffer containing 300 mM KCl. Proteins in each elute were analyzed by electrophoresis on 10% NuPAGE Novex Bis-Tris gel (Invitrogen). Binding activity of each elute was evaluated by gel shift assay.

In-gel digestion

Protein bands were excised from a silver-stained gel. Proteins were digested with sequencing grade-modified trypsin (Roche Diagnostics) as described elsewhere.[19] Tryptic peptides were extracted from gel pieces in 50% acetonitrile with 5% formic acid and dried using a vacuum centrifuge. Dried peptides were resuspended in 5% acetonitrile containing 0.1% trifluoroacetic acid and desalted using StageTips with a C18 Empore disk membrane (3M, Minneapolis, MN, USA) according to the published procedure.[20]

Liquid chromatography-tandem mass spectrometry (LC-MS/MS) and data analysis

LC-MS/MS analysis was performed using a Paradigm MS4 nanoHPLC system (Michrom BioResources, Inc., Auburn, CA, USA) coupled to a LTQ linear ion trap mass spectrometer (Thermo Electron Corp., Waltham, MA, USA) with a

nanoelectrospray ionization source (AMR Inc., Tokyo, Japan). Tryptic peptides were injected by a HTC-PAL autosampler (CTC Analytics, Zwingen, Switzerland) and enriched on a C18 trap column (300 μm I.D. × 5 mm length, CERI, Tokyo, Japan) at a flow rate of 6 μl min^{-1}. The samples were subsequently separated by a C18 reverse phase column (100 μm I.D. × 150 mm length, Nikkyo Technos, Tokyo, Japan) at a flow rate of 1 μl min^{-1}, with a linear gradient from 2% to 65% mobile phase B, that is; from 98% to 35% of mobile phase A. The mobile phase B consisted of 95% acetonitrile with 0.1% formic acid, whereas the mobile phase A consisted of 2% acetonitrile with 0.1% formic acid. LC-MS/MS analysis was carried out using a data-dependent triple-play mode. Automated gain control values were set at 1.5×10^4, 1.5×10^3 and 5.0×10^3 for Full-MS, Zoom-MS and MS/MS, respectively. A spray voltage of 2.4 kV was applied. The MS scan range was *m/z* 300–2000. Peptides and proteins were identified by Mascot software ver. 2.2 (Matrix Science, London, UK), screened against the most recent version of the human IPI database from EMBL-EBI (http://www.ebi.ac.uk/IPI/IPIhuman.html). Maximum tolerance was set to 1.2 Da for MS data, 0.5 Da for MS/MS data and strict trypsin specificity allowing for up to one missed cleavage. Carbamidomethylation of cysteine and oxidation of methionine were allowed as variable modifications.

Transfection of YY1

SH-SY5Y cells were transfected with pCMV6-XL5 expressing human YY1 (OriGene, Rockville, MD, USA) or blank vector by using an electroporator CUY21 *Pro-Vitro* (NEPA GENE, Chiba, Japan). Twenty-four hours after transfection, the cells were harvested. For western blotting, whole-cell lysates were separated by electrophoresis on 10% NuPAGE Novex Bis-Tris gel and blotted onto PVDF membrane (Immobilon-P, Merck Millipore, Darmstadt, Germany). The membranes were incubated with anti-YY1 (sc-1703, Santa Cruz Biotechnology, Santa Cruz, CA, USA) or anti-Actin (sc-10731, Santa Cruz Biotechnology), followed by reaction with horseradish peroxidase-conjugated secondary antibodies. Signal detection was performed using the ECL detection system (Thermo Fisher Scientific, Rockford, IL, USA).

Overexpression/knockdown of *RP11-115D19.1*

For overexpression experiment, *RP11-115D19.1-003* cDNA (469 bp) was amplified from SH-SY5Y cDNA and *RP11-115D19.1-005* cDNA (567 bp) was synthesized (Genscript, Piscataway, NJ, USA). Each fragment was cloned into pCMV6-XL5 and transfected to SH-SY5Y cells as described above. For repression experiment, siRNA targeting to *RP11-115D19.1* (5′-CATGCTTC-CAGAGAATGCATATTCT-3′) was designed from the common region between *RP11-115D19.1-003* and *-005*. The siRNA and negative control (Lo GC duplex) were purchased (Stealth RNAi, Invitrogen) and transfected as described above. Twenty-four hours after transfection, the cells were harvested.

Real-time reverse transcription-PCR (RT-PCR)

As described previously, autopsied frontal cortices were obtained from the Brain Bank for Aging Research (Tokyo Metropolitan Geriatric Hospital/Tokyo Metropolitan Institute of Gerontology) and Department of Neurology, Juntendo University School of Medicine, Tokyo, Japan. The samples contained 21 cases (age, 82.6 ± 7.1 (s.d.) years; 11 males and 10 females) with Lewy body pathology defined by the third Consensus Guideline for Dementia with Lewy Bodies, comprising PD with and without dementia and DLB and 18 control subjects (age, 81.2 ± 5.2 years; 12 males and 6 females) without parkinsonism or dementia and without neurodegenerative pathological changes. Total RNA was extracted from SH-SY5Y cells or tissue using RNeasy (Qiagen), and cDNA was prepared using High Capacity RNA-to-cDNA kit (Applied Biosystems). Real-time RT-PCR was carried out on StepOnePlus real-time PCR system (Applied Biosystems) using Fast SYBR Green Master Mix (Applied Biosystems). First-strand cDNA was amplified using primers specific for *SNCA* (forward; 5′-CAGAAGCAGCAGGAAAGACA-3′, reverse; 5′-CCACTGCTCCT CCAACATTT-3′, product size; 132 bp), *RP11-115D19.1-003* (forward; 5′-TAA AACCTGCAAATTCACATCTTC-3′, reverse; 5′-AAGTAGGTAAGTAGGGCAG TGCAT-3′ product size; 133 bp), *RP11-115D19.1-005* (forward; 5′-CCATGCTT CCAGAGAATGCA-3′, reverse; 5′-GTGCTTCCCTTTCACTGAAG-3′, product size; 144 bp), *GAPDH* (forward; 5′-CATCTTCCAGGAGCGAGATC-3′, reverse; 5′-TGCAAATGAGCCCCAGCCTT-3′, product size; 114 bp), *NF* (*neurofilament L*, forward; 5′-AAGAACACCGACGCCGTGCG-3′, reverse; 5′-TGCCATTTCACTCTTTGTGG-3′, product size; 222 bp), and *YY1* (forward; 5′-TGGCAAAGCTTTTGTTGAGA-3′, reverse; 5′-ATGTGTGCGCAAATTGA AGT-3′, product size; 130 bp). For quantification, we used a relative standard curve method and amplified cDNA corresponding to 100 ng (*RP11-115D19.1*) or 1.7 ng (*SNCA*, *GAPDH*, and *NF*) RNA per well. Standard curves were generated from amplification of diluted series of cDNA from cortices (*SNCA*, *GAPDH*, and *NF*), YY1-transfected SH-SY5Y cells (*RP11-115D19.1*) or plasmids (pCMV-YY1, pCMV-RP11-115D19.1-003, pCMV-RP11-115D19.1-005). *SNCA*, *RP11-115D19.1* and *YY1* expression levels were normalized to those of *GAPDH* (SH-SY5Y cells) or *NF* (cortices). The values were determined in triplicate or duplicate. Genotyping of rs356219 of SH-SY5Y and cortices was performed using restriction fragment length polymorphism and sequencing.

RESULTS

Identification of four *SNCA* SNPs associated with PD in both the Japanese and European populations

We previously identified six SNPs (rs3857053, rs356165, rs7684318, rs3775424, rs3796661 and rs2737029), located in the 3′-flanking, 3′-UTR and intron 4 of *SNCA*, that were prominently associated with PD.[13] Independently, analysis of a European population also reported

Table 1 PD-associated *SNCA* SNPs reported in the Japanese and German studies

	Position	Region	Japanese study[a]		German study[b]		MAF of Europeans in the dbSNP database		
SNP ID	(NCBI build 36)		P-value	MAF (Case/control)	P-value	MAF (Case/control)	HapMap-CEU	EGP_CEPH_PANEL	AFD_EUR_PANEL
rs356219	90637601	3′-Flanking	7.3×10^{-9}	0.34/0.43	0.00467	0.46/0.38	0.425		0.354
rs356220	90641340	3′-Flanking	8.7×10^{-10}	0.33/0.43	0.00485	0.46/0.38	0.427		
rs3857053	90645674	3′-Flanking	1.1×10^{-9}	0.33/0.43				0.071	
rs356165	90646886	3′-UTR	2.0×10^{-9}	0.33/0.43	0.00555	0.46/0.38	0.433	0.412	
rs7684318	90655003	Intron 4	5.0×10^{-10}	0.33/0.43					0.024
rs3775424	90665256	Intron 4	5.4×10^{-10}	0.33/0.43			0.033		
rs356203	90666041	Intron 4	1.4×10^{-7}	0.34/0.43	0.00548	0.46/0.38		0.45	
rs3796661	90687507	Intron 4	2.7×10^{-9}	0.33/0.42			0.033		0.021
rs2737029	90711770	Intron 4	1.7×10^{-11}	0.32/0.42	0.09994	0.46/0.42	0.45		0.396

Abbreviations: MAF, minor allele frequency; NCBI, National Center for Biotechnology Information; PD, Parkinson's disease; *SNCA*, *α-synuclein*; SNP, single-nucleotide polymorphism; UTR, untranslated region.
[a]From our previous study[13] and present study (rs356219, rs356220 and rs356203).
[b]From the previous German study[12] (replication sample set II).

strong association for four SNPs (rs356219, rs356220 rs356165, rs356203) in the 3′-flanking region of *SNCA*.[12] Of these SNPs, only rs356165 was common to the two studies. We genotyped the remaining SNPs of the European population (rs356219, rs356220 and rs356203) and confirmed their prominent association with the Japanese population (Table 1, Figure 1a). The remaining SNPs reported in the Japanese population study were rare in the European population (Table 1, Figure 1a). From these findings, we concluded that rs356219, rs356220, rs356165 and rs356203 were associated prominently with PD in both the populations. Our functional analysis focused on these four SNPs.

Allele-specific effect of rs356219 in luciferase and gel shift assays

To determine whether the four SNPs could affect *SNCA* expression levels, we constructed plasmids containing genomic fragments with each SNP, placed downstream from a luciferase transcriptional unit (Figure 1b). For rs356219, the clone containing the protective A allele showed 1.6-fold greater luciferase activity than did the disease-associated G allele. We observed no allele-specific differences for the remaining three SNPs, however. Next, we used gel shift assays to examine the possibility that proteins might bind to the SNPs in an allele-specific manner (Figure 1c). The protective rs356219-A allele showed an intense shift band relative to the disease allele rs356219-G. Alleles of rs356220 and rs356165 showed similar shift band intensities. For rs356203, the intensity of the C disease allele was stronger than that of the protective T allele. We focused our subsequent analyses on rs356219, which was the only SNP that showed allele-specific features in both the assays.

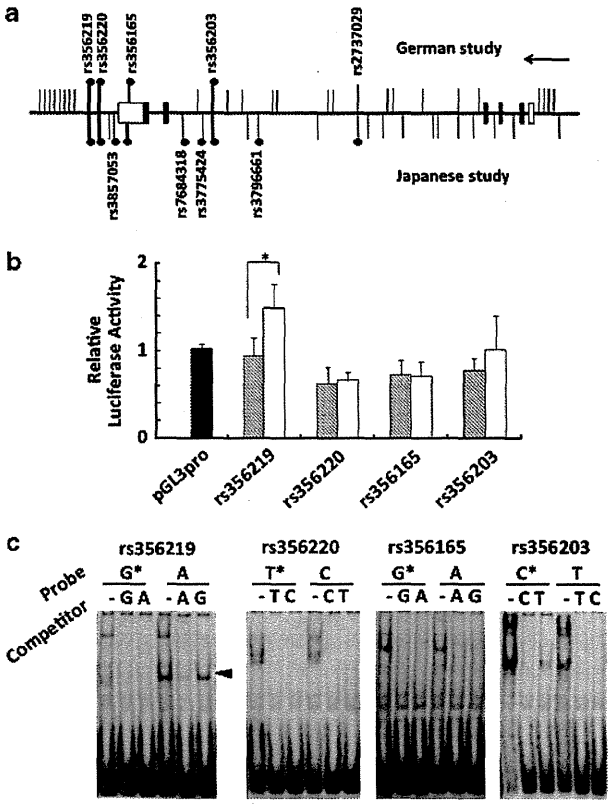

Figure 1 Transcriptional regulatory activity affected by *SNCA* SNPs. (**a**) Schematic representation of the *SNCA* gene with relative positions of SNPs genotyped in the Japanese and European population studies. The *SNCA* locus (horizontal line), coding regions (black boxes), 5′- and 3′-UTR (white boxes) and transcription orientation (arrow) are shown. The relative positions of SNPs (vertical lines) genotyped in the Japanese study (lower) and the German study (upper) are represented. Of the SNPs strongly associated with each study (solid circle), four SNPs are commonly associated with PD in both the studies (thick vertical lines). (**b**) Luciferase assay. Luciferase activities relative to the control pGL3-promoter construct (black bar) were compared between disease allele (shaded) and protective allele (white) at each of the four SNPs ($n=7$). Luciferase activity of the protective rs356219-A allele was significantly increased relative to that of the G disease allele (*$P=0.001$ by Student's *t*-test). (**c**) Gel shift assay. Binding of SH-SY5Y nuclear protein to alleles at the four SNPs are presented. Shift bands were compared between the disease allele (*) and the protective allele at each SNP. The intense shift band observed for the protective allele rs356219-A was competed by non-labeled competitor allele A but not by the disease allele G (arrowhead).

Identification of the rs356219-A binding protein

We performed UV-crosslinking and estimated the size of the protein bound to the rs356219-A allele at ~55 kDa (Figure 2a). Next, we purified the protein by binding to rs356219-A affinity beads in the presence of non-biotinylated rs356219-G fragments as a competitor. Control experiments used non-biotinylated rs356219-A fragments as competitor. After washing, the binding protein was eluted sequentially, twice with elution buffer containing 200 mM KCl and twice with buffer containing 300 mM KCl. Electrophoresis and gel shift assay located the ~55 kDa band and binding activity within the second (200 mM KCl) and third (300 mM KCl) elutes. Both were absorbed by the rs356219-A competitor in the control experiments (Figure 2b). Subsequent LC-MS/MS analysis showed that peptides derived from a transcription factor YY1 were identified from the ~55 kDa bands (Figure 2c). We concluded that the rs356219-A binding protein was YY1. This observation was confirmed by super-shift assays using anti-YY1 antibody (Figure 2d, Supplementary Figure 1).

Effects of YY1 transfection on *SNCA* and noncoding RNA (ncRNA) *RP11-115D19.1* expression in SH-SY5Y cells

Luciferase assay and gel shift assay suggested that YY1 bound to rs356219 protective allele and stimulated transcription (Figures 1b and c and 2). Recent Ensemble Genome Browser showed antisense ncRNA named *RP11-115D19.1* in *SNCA* 3′-flanking region. The SNP rs356219 locates intron of its two spliced isoforms (*RP11-115D19.1-003* and *-005*; Figure 3a), suggesting that rs356219 might influence transcription of *SNCA* and/or *RP11-115D19.1*. If rs356219 influences *SNCA* promoter, increased luciferase activity in the protective allele (Figure 1b) appears incompatible with the hypothesis that increased SNCA leads to PD. To address this issue, we investigated YY1-induced expression of *SNCA* and *RP11-115D19.1* in SH-SY5Y neuroblastoma cells, whose genotype of rs356219 was heterozygous. YY1 transfection showed 23-fold increase in *RP11-115D19.1-003*, 24-fold increase in *RP11-115D19.1-005* and twofold increase in *SNCA* expression levels (Figure 3b). Other two independent transfection experiments replicated the prominent stimulation of *RP11-115D19.1* by YY1; however, they showed little changes of *SNCA* expression (data not shown). We analyzed allele-specific expression level of *SNCA* by using 3′-UTR SNP rs356165 as a marker and found little difference between the alleles, both in YY1 and blank transfection (Figure 3c). We could not analyze allele-specific expression of *RP11-115D19.1*, because no SNP was found in *RP11-115D19.1* exons in SH-SY5Y. Although the role of *RP11-115D19.1* on *SNCA* expression remains uncovered, increased luciferase activity in the

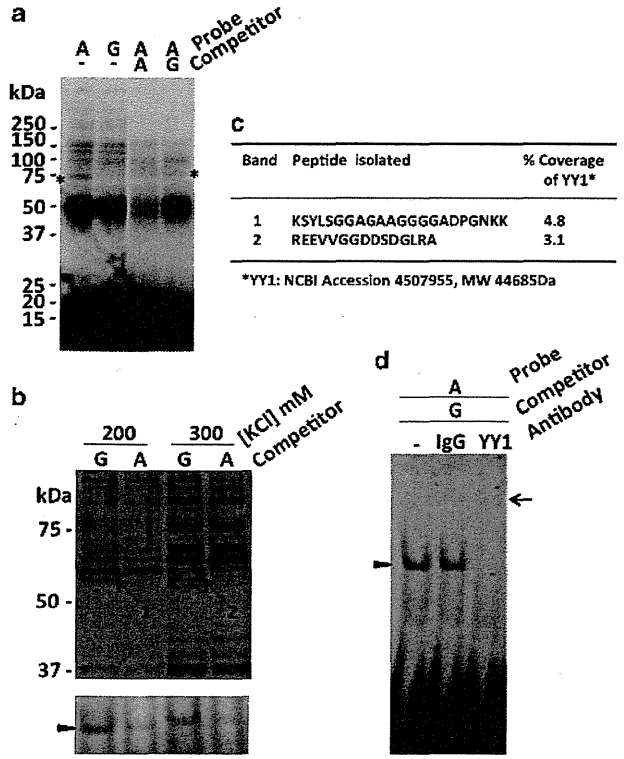

Figure 2 Purification and identification of the rs356219-A binding protein. (**a**) Estimation of the molecular size of the rs356219-A binding protein by UV cross-linking analysis. SH-SY5Y nuclear extract was incubated with the probe, rs356219-A (protective allele) or rs356219-G (disease allele) in the presence or absence of non-labeled competitor. Following UV irradiation, the cross-linked protein–probe complexes were analyzed by SDS-PAGE. The size of allele A and protein complex was estimated as ~70 kDa (*). As the mean size of the free probe was estimated as ~15 kDa, the protein of interest was estimated as ~55 kDa. (**b**) Purification of the rs356219-A binding protein using DNA affinity beads. Nuclear extract from SH-SY5Y cells was incubated with affinity beads bound to tandem repeats of 33 bp region containing the A allele, in the presence of free competitor G allele (for purification) or control allele A. After the binding reaction, beads were washed and eluted twice with buffer containing 200 mM KCl and then twice with buffer containing 300 mM KCl. Aliquots of each elution were analyzed by SDS-PAGE (upper panel) and gel shift assays using rs356219-A as a probe (lower panel). The second and third elutions are shown. The rs356219-A binding band of ~55 kDa was observed (bands 1 and 2, arrows) and correlated with the intensity of the gel shift band (arrowhead). (**c**) Summary of mass spectrometry analysis of the two ~55 kDa bands. Peptides derived from YY1 were identified from both bands. (**d**) Supershift assay using anti-YY1 antibody. After binding of the rs356219-A probe and SH-SY5Y nuclear extract in the gel shift assay, anti-YY1 antibody was added and analyzed by electrophoresis. The shift band (arrowhead) was supershifted by anti-YY1 antibody (arrow), confirming that the shift band contains YY1.

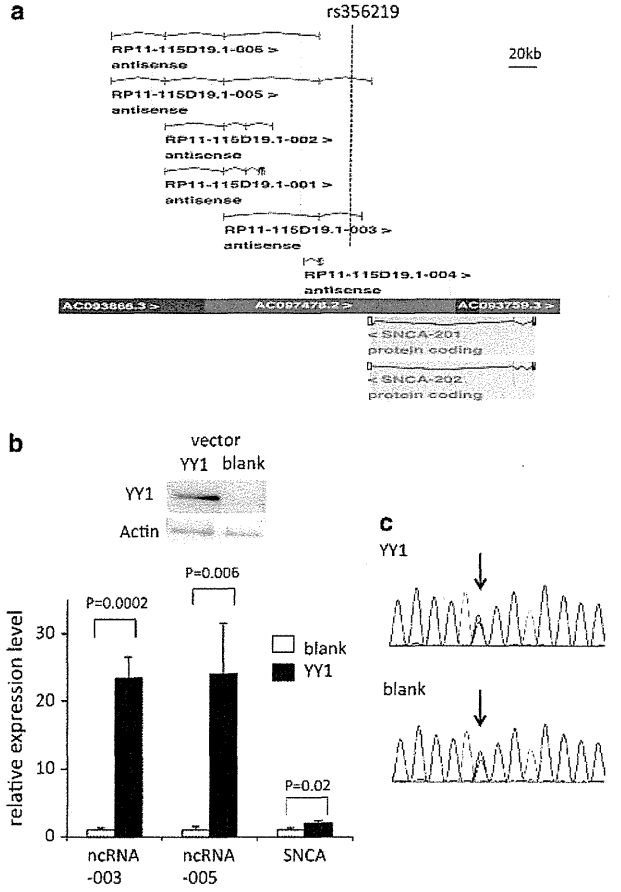

Figure 3 *SNCA* and its 3′-flanking ncRNA expression in YY1-transfected SH-SY5Y cells. (**a**) Genomic structure of *SNCA* and its 3′-flanking region (Ensemble Genome Browser). SNP rs356219 locates in intron of *RP11-115D19.1-003* and *-005* (dotted line). (**b**) Quantification of *SNCA* mRNA and two spliced isoforms of *RP11-115D19.1* ncRNA (*-003* and *-005*) in SH-SY5Y cells transfected by YY1 expression vector or blank vector. Overexpression of YY1 was confirmed by western blot analysis (upper). Three YY1 plates and three blank plates were quantified. Mean values of three YY1 plates (black bar) relative to the mean of three blank plates (white bar) are shown with s.d. (lower). YY1 transfection showed 23-fold increase in *RP11-115D19.1-003*, 24-fold increase in *RP11-115D19.1-005* and twofold increase in *SNCA* expression levels. (**c**) Semiquantitative analysis of allele-specific expression of *SNCA* 3′-UTR. Sequencing chromatograms of SH-SY5Y RT-PCR products of *SNCA* 3′-UTR containing rs356165 (arrow) are shown. Little difference between the heights of allele-C and allele-T was observed, both in the YY1 and blank transfection.

protective allele is not contradictory to YY1-stimulated expression of *RP11-115D19.1*.

SNCA, ncRNA *RP11-115D19.1* and *YY1* expression in relation to rs356219

We found the possibility that rs356219 may influence expression of *RP11-115D19.1* from *in vitro* and cellular experiments (Figures 1–3). To extend the findings, we investigated *SNCA* and *RP11-115D19.1* expression in relation to rs356219 genotypes in autopsied brain tissues. We previously reported that *SNCA* expression levels tended to be positively correlated with the number of the disease allele of rs7684318 in autopsied cortices.[13] Because rs356219 and rs7684318 are in a tight linkage disequilibrium group (Supplementary Table 3), our previous finding is to be replicated in relation to rs356219. Actually, rs356219 genotypes were completely correlated with those of rs7684318 in our autopsied samples. Moreover, we synthesized new cDNAs and quantified *SNCA* expression levels by real-time RT-PCR to compare among rs356219 genotypes. Although the difference among genotypes did not reach significance, we confirmed similar tendency with our previous report; mean of *SNCA* mRNA was lowest in AA (homozygote of protective alleles) either in cases, controls and combined (Supplementary Figure 2a). We also analyzed *RP11-*

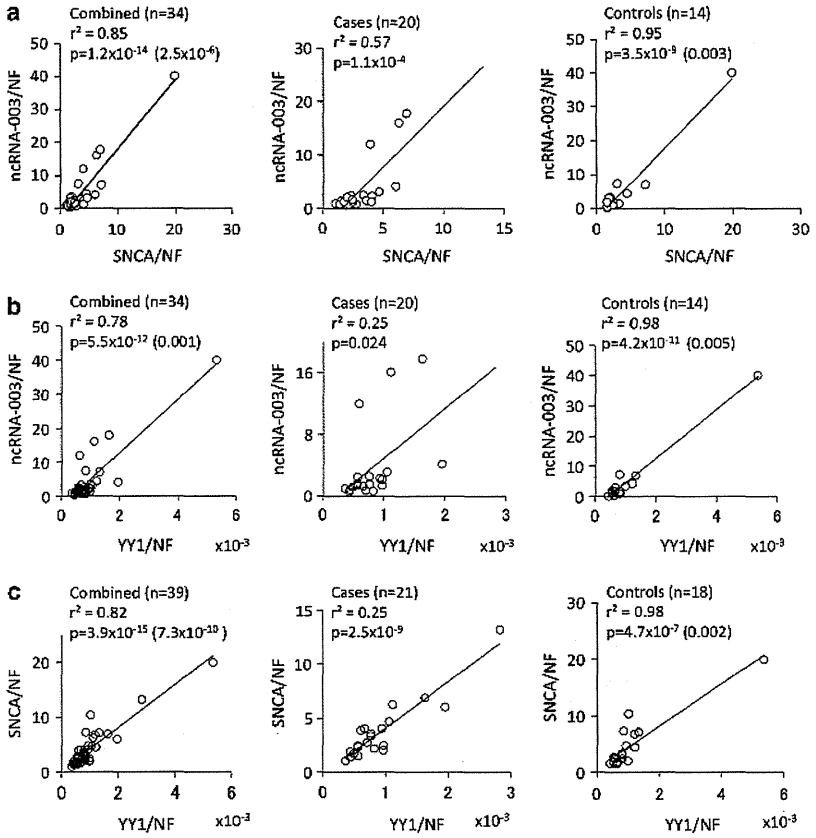

Figure 4 Correlation of SNCA, its 3′-flanking ncRNA and YY1 expression levels in autopsied frontal cortices. Scatterplots of *SNCA* versus *RP11-115D19.1-003* (**a**), *YY1* versus *RP11-115D19.1-003* (**b**) and *YY1* versus *SNCA* (**c**) expression levels (standardized by NF in arbitrary units). Plots are shown in all the samples (combined), cases and controls separately. Linear regression lines are indicated with r^2 and *P* values (Pearson's correlation analysis). Even after excluding the outliner in the controls, the strong correlations remain (*P*-values are in parenthesis).

115D19.1 expression in relation to rs356219. *RP11-115D19.1-005* expression levels in 38 out of the 39 cortices were too low to be quantified (data not shown); however, those of *RP11-115D19.1-003* could be quantified in 34 cortices. Compared with *SNCA*, mean values of *RP11-115D19.1-003* expression levels showed little difference among rs356219 genotypes (Supplementary Figure 2b). However, it was notable that *RP11-115D19.1-003* expression levels were strongly and positively correlated with those of *SNCA* (Figure 4a). Even after excluding the outliner in the controls, the strong correlation remained ($P = 2.5 \times 10^{-6}$ in combined and $P = 0.003$ in controls). We also examined *YY1* mRNA expression levels in cortical tissues. *YY1* expression levels were normalized by those of *NF*, because previous immunohistochemical study in an adult rodent brain reported that YY1 were strongly expressed in neurons and not detected in astrocytes.[21] *YY1* expression levels showed no significant difference among rs356219 genotype (Supplementary Figure 2c); however, positive correlation between *YY1* and *RP11-115D19.1-003* (Figure 4b) was compatible to the YY1-induced ncRNA expression shown in cellular YY1-overexpression experiment (Figure 3).

Effects of overexpression/knockdown of ncRNA *RP11-115D19.1* on *SNCA* expression in SH-SY5Y cells

Positive correlation between *SNCA* and *RP11-115D19.1* in the brain suggests regulatory roles of *RP11-115D19.1* on the *SNCA* expression. To address this issue, we investigated *SNCA* expression levels in SH-SY5Y cells transfected by *RP11-115D19.1* expressing vectors or siRNA designed from a common region of *RP11-115D19.1-003* and *-005*. Overexpression of *RP11-115D19.1* did not affect *SNCA* expression levels significantly (Figure 5a). On the contrary, siRNA-mediated knockdown (~90%) of *RP11-115D19.1* increased *SNCA* expression levels significantly (1.2-fold, $P = 0.0014$) (Figure 5b), which was replicated in three independent knockdown experiments (data not shown). These findings suggest that *RP11-115D19.1* may have repressive effect on the *SNCA* expression.

DISCUSSION

Recent GWAS have provided new information regarding PD susceptibility genes.[14,15] Our GWAS analysis in the Japanese population confirmed strong associations at *SNCA* and *LRRK2* and identified novel susceptibility loci, including *PARK16* (1q32) and *BST1* (4p15).[14] GWAS in individuals of European ancestry confirmed strong associations at *SNCA*, *MAPT* and *LRRK2*, and also confirmed *PARK16* as a novel locus.[15] Following meta-analysis of GWAS in the European ancestry populations confirmed *BST1* susceptibility.[22] Susceptibility associated with *MAPT* was not consistent between the populations, in part because of ethnic differences in allele frequencies. For example, a strong association for the H1/H2 haplotype of *MAPT* (OMIM 157140) has been reported in Caucasians,[23] but this observation has not been replicated in Asians. The frequency of the H2 haplotype is

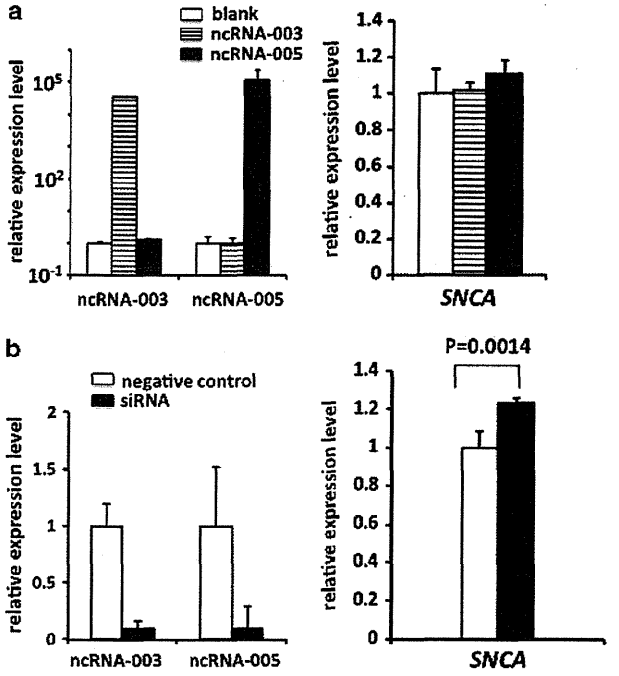

Figure 5 *SNCA* expression in SH-SY5Y cells after overexpression/knockdown of the ncRNA. (**a**) Quantification of *SNCA* mRNA in SH-SY5Y cells transfected by *RP11-115D19.1 ncRNA-003* and *-005* expression vectors or blank vector. Mean values of three *ncRNA-003* plates (striped bar) or three *ncRNA-005* (black bar) plates relative to the mean of three blank plates (white bar) are shown with s.d. Overexpression (over 10000-fold) of *ncRNA-003/-005* was confirmed (left). *SNCA* expression did not change significantly by transfection of *ncRNA-003* ($P=0.83$, versus blank, *t*-test) or *ncRNA-005* ($P=0.28$, versus blank, *t*-test) (right). (**b**) Quantification of *SNCA* mRNA in SH-SY5Y cells transfected by siRNA targeted to *RP11-115D19.1* or negative control RNA. Mean value of four siRNA plates (black bar) relative to the mean of four control plates (white bar) are shown with s.d. Repression of the *ncRNA-003/005* (~0.1-fold) was confirmed (left). *SNCA* expression increased significantly (~1.2-fold, $P=0.0014$, *t*-test) by transfection of siRNA (right).

approximately 20% in Caucasians but almost absent in Asians.[24] On the contrary, *SNCA*, *LRRK2*, *BST1* and *PARK16* susceptibilities are consistent in both the populations. To examine how SNPs might affect disease susceptibility, we focused on the *SNCA* SNPs that associate with PD across different ethnicities.

Of the four SNPs analyzed, only rs356219 showed distinct allele-specific features. The protective A allele showed greater activity in lucifersae assays than did the disease allele G. Moreover, specific binding of a nuclear protein to the protective A allele was observed using gel shift assays. When purified, this protein was identified as the transcription factor YY1, a ubiquitous zinc-finger transcription factor belonging to the Drosophila-Polycomb group protein family. The name Yin Yang 1 reflects its dual effects on transcriptional regulation, as YY1 can stimulate or repress gene expression depending on the cellular context. YY1 is associated with multiple biological functions such as proliferation, differentiation, apoptosis and tumorigenesis.[25,26] Comparison with known YY1 consensus binding motifs[27] supports the idea that the sequence of rs356219 would alter YY1 affinity in an allele-specific manner (Supplementary Figure 1). Based on the hypothesis that increased SNCA leads to LBD, it is reasonable to presume that YY1 could diminish *SNCA* gene expression levels by binding to the protective allele. However, elevated luciferase activity of the construct containing the rs356219-A protective allele seems contradictory. To address this issue, we transfected YY1 expression vector to human neuroblastoma cell line SH-SY5Y of which rs356219 genotype is GA and compared allele-specific expression level using 3′-UTR SNP rs356165 as a marker. YY1 was successfully overexpressed in SH-SY5Y and little difference of *SNCA* expression levels between the alleles was observed (Figure 3c), suggesting little possibility of allele-specific transcription regulation by YY1–rs356219 interaction, at least in SH-SY5Y cells. We raised another possibility that rs356219 might influence transcription of a certain gene regulating *SNCA* expression. Recent Ensemble Genome Browser (http://www.ensembl.org/) showed novel antisense ncRNA *RP11-115D19.1* in *SNCA* 3′-flanking region. We also investigated the expression of *RP11-115D19.1*, because rs356219 is located in introns of the two spliced isoforms, *RP11-115D19.1-003* and *-005* (Figure 3a). Surprisingly, *RP11-115D19.1* expression was prominently stimulated by YY1 overexpression, in contrast to the little change in *SNCA* expression (Figure 3b). From these findings, it would be informative to analyze *RP11-115D19.1* expression levels stimulated by YY1 in relation to rs356219 genotypes. Because no SNP was found in SH-SY5Y *RP11-115D19.1* exons, we designed an experiment to transfect YY1 expression vector to human lymphoblasts G or A in rs356219 and compare *SNCA* mRNA expression levels between G and A. However, because of low transfection efficiency (~10% by electroporation), we could not induce YY1 in lymphoblasts (data not shown).

Our *in vitro* and cellular experiments showed the possibility that rs356219 might influence YY1-stimulated transcription of *RP11-115D19.1*. To extend this, we investigated steady state *SNCA* and *RP11-115D19.1* expression levels in autopsied frontal cortices in relation to rs356219 genotypes. *SNCA* expression levels in cortices tended to be positively correlated with the number of the disease allele of rs356219 (Supplementary Figure 2a), replicating our previous result.[13] Our result was not consistent with other groups' previous reports. Fuchs *et al.*[28] reported that higher *SNCA* mRNA correlated with rs356219 disease allele in the substantia nigra of the midbrain, however, with the protective allele in the cerebellum. On the other hand, Linnertz *et al.*[29] reported that higher *SNCA* mRNA correlated with rs356219 protective allele in the temporal cortices and midbrain and unchanged among the genotypes in the frontal cortices. The discrepancies among these studies might be from the number and variation of samples.

We also analyzed steady state *in vivo RP11-115D19.1* expression levels and found little difference among genotypes (Supplementary Figure 2b). However, it was of note that *RP11-115D19.1* expression levels were strongly and positively correlated with those of *SNCA* (Figure 4a). Recent reports focused on SNP-coexpression associations.[30,31] We found a positive correlation between *SNCA* and *RP11-115D19.1* in either of the rs356219 genotype. The significance of correlation tended to increase according to the number of the disease allele G (Supplementary Figure 3). To confirm this tendency, large number of samples must be analyzed.

We also quantified *RP11-115D19-003* and *SNCA* mRNA levels in lymphoblasts originated from PD patients harboring GG and AA (Supplementary Figure 4). Similarly to the brain, there were no significant differences in *RP11-115D19-003* and *SNCA* expression levels between GG and AA lymphoblasts. In contrast to the brain, however, there was no significant correlation between *RP11-115D19-003* and *SNCA* levels in lymphoblasts. Although the numbers examined were limited, these results suggest interaction between *RP11-115D19* and *SNCA* expressions may be brain-specific.

The coexpression suggests functional interaction between the two genes. *RP11-115D19.1* transcripts span 0.4–1.8 kb, classified by size to long noncoding RNAs (lncRNAs).[32] Although the function of majority of lncRNAs remains uncovered, some are supposed to participate in regulating transcription of coding genes. For example, it was reported that mRNA of *BACE1*, *β-site APP (amyloid precursor protein) cleaving enzyme 1*, was stabilized by *BACE1* antisense transcript, a lncRNA including an exon complementary to a *BACE-1* exon.[33] On the contrary, recent work reported that *brain-derived neurotrophic factor* (*BDNF*) was repressed by its antisense RNA transcript.[34] These reports showed that some antisense ncRNAs downregulated and others upregulated transcription of the sense genes. *RP11-115D19.1-005* transcript overlaps *SNCA* 3′-UTR partly in tail-to-tail manner (Figure 3a), suggesting putative regulatory activity on *SNCA* expression. *RP11-115D19.1-005* transcript was hardly detected in steady state brain mRNA; however, it was prominently stimulated by YY1 in SH-SY5Y cells, as well as in *-003* transcript.

To investigate how *RP11-115D19.1* may influence *SNCA* expression, we performed cellular overexpression and knockdown experiments. We found that siRNA-mediated knockdown of the ncRNA increased *SNCA* expression (~ 1.2-fold) in SH-SY5Y cells (Figure 5b). The effect seems small; however, it could be sufficient to influence susceptibility to late-onset sporadic PD and DLB, caused by multiple genetic and environmental factors. The reason why overexpression of the ncRNA did not suppress *SNCA* expression remains unknown. We hypothesize that ncRNA may influence *SNCA* expression in a locus-dependent manner and that repressive effect may be saturated at endogeneous (low) expression level of ncRNA.

We performed similar analysis using human embryonic kidney-derived HEK293 cells. YY1-induced expression of ncRNA was replicated in HEK293 cells (Supplementary Figure 5). The degree of ncRNA stimulation in HEK293 cells, however, was smaller than those in SH-SY5Y cells. *SNCA* expression levels in HEK293 cells did not change significantly after YY1 overexpression, ncRNA overexpression or ncRNA knockdown. These suggest that ncRNA's repressive effect on *SNCA* expression may be specific to neuroblastoma cells.

Based on our demonstration that ncRNA has directly repressive effect on *SNCA* expression *in vitro*, positive correlation between *SNCA* and its antisense ncRNA *in vivo* may be explained as follows: One possibility is that expression of antisense ncRNA may coordinate with that of sense gene *SNCA* under locus-specific transcriptional regulation. Another possibility is that certain neurotoxic factors, including oxidative stress, may cause stimulation of *SNCA* and ncRNA expression levels simultaneously. Simultaneous stimulation of *SNCA* and *YY1* may be also possible, because of correlation of *SNCA* and *YY1* expression levels in the brain (Figure 4c) and YY1-induced expression of ncRNA in cells (Figure 3). In both the hypotheses (Supplementary Figure 6), ncRNA may be beneficial to maintain *SNCA* expression levels within normal range.

Accumulation of SNCA is thought to be neurotoxic. On the other hand, the protective effects of SNCA are also reported. Chandra *et al.*[35] reported that transgenic expression of *SNCA* rescued neurodegeneration in *CSPα* knockout mice. Musgrove *et al.*[36] reported that endogeneous SNCA upregulation in response to weak oxidative stress was neuroprotective against additional acute oxidative stress in primary cultured neurons. These suggest that SNCA exerts neuroprotective effects under disease or stress. However, repeated stresses or lasting disease state may cause SNCA accumulation. Extraordinary upregulation of SNCA may be also harmful. Therefore, *SNCA* expression levels must be fine-tuned to maintain proper range *in vivo*. To clarify the regulatory mechanism of the ncRNA, with or without neurotoxic stresses, further intensive approach should be necessary.

In conclusion, our findings of the protective-allele specific YY1 and antisense ncRNA raised a novel possible mechanism to regulate *SNCA* expression.

CONFLICT OF INTEREST

The authors declare no conflict of interest.

ACKNOWLEDGEMENTS

We are grateful to the individuals with PD who participated in this study. We also thank Dr Yoshitaka Nagai for helpful comments; Dr Kouichi Ozaki for technical comments of luciferase assay and gel shift assay; Dr Fumiko Hirose and Dr Isao Kuraoka for technical comments of protein purification by affinity beads; Dr Hidetoshi Inoko and Dr Katsushi Tokunaga for control samples; Dr Yoshihisa Watanabe for technical comments of electroporation; and Dr Jennifer Logan for editing the manuscript. This work was supported by a grant from the Core Research for Evolutional Science and Technology (CREST), Japan Science and Technology Agency (JST); by the Global COE program and KAKENHI (17019044 and 19590990), both from the Ministry of Education, Culture, Sports, Science and Technology of Japan; and by the Grant-in-Aid for 'The Research Committee for the Neurodegenerative Diseases' of the Research on Measures for Intractable Diseases and Research Grant (H19-Genome-Ippan-001), all from the Ministry of Health, Labor and Welfare of Japan.

1 de Rijk, M. C., Tzourio, C., Breteler, M. M., Dartigues, J. F., Amaducci, L., Lopez-Pousa, S. *et al.* Prevalence of parkinsonism and Parkinson's disease in Europe: the EUROPARKINSON Collaborative Study. European Community Concerted Action on the Epidemiology of Parkinson's disease. *J. Neurol. Neurosurg. Psychiatry* **62,** 10–15 (1997).
2 Shults, C. W. Lewy bodies. *Proc. Natl Acad. Sci. USA* **103,** 1661–1668 (2006).
3 Farrer, M. J. Genetics of Parkinson disease: paradigm shifts and future prospects. *Nat. Rev. Genet.* **7,** 306–318 (2006).
4 Lesage, S. & Brice, A. Parkinson's disease: from monogenic forms to genetic susceptibility factors. *Hum. Mol. Genet.* **18,** R48–R59 (2009).
5 Warner, T. T. & Schapira, A. H. Genetic and environmental factors in the cause of Parkinson's disease. *Ann. Neurol.* **53** (Suppl 3), S16–S23 (2003).
6 Polymeropoulos, M. H., Lavedan, C., Leroy, E., Ide, S. E., Dehejia, A., Dutra, A. *et al.* Mutation in the α-synuclein gene identified in families with Parkinson's disease. *Science* **276,** 2045–2047 (1997).
7 Spillantini, M. G., Schmidt, M. L., Lee, V. M., Trojanowski, J. Q., Jakes, R. & Goedert, M. α -Synuclein in Lewy bodies. *Nature* **388,** 839–840 (1997).
8 Singleton, A. B., Farrer, M., Johnson, J., Singleton, A., Hague, S., Kachergus, J. *et al.* α -Synuclein locus triplication causes Parkinson's disease. *Science* **302,** 841 (2003).
9 Miller, D. W., Hague, S. M., Clarimon, J., Baptista, M., Gwinn-Hardy, K., Cookson, M. R. *et al.* α-Synuclein in blood and brain from familial Parkinson disease with *SNCA* locus triplication. *Neurology* **62,** 1835–1838 (2004).
10 Chartier-Harlin, M. C., Kachergus, J., Roumier, C., Mouroux, V., Douay, X., Lincoln, S. *et al.* α-Synuclein locus duplication as a cause of familial Parkinson's disease. *Lancet* **364,** 1167–1169 (2004).
11 Ibanez, P., Bonnet, A. M., Debarges, B., Lohmann, E., Tison, F., Pollak, P. *et al.* Causal relation between α-synuclein gene duplication and familial Parkinson's disease. *Lancet* **364,** 1169–1171 (2004).
12 Mueller, J. C., Fuchs, J., Hofer, A., Zimprich, A., Lichtner, P., Illig, T. *et al.* Multiple regions of α-synuclein are associated with Parkinson's disease. *Ann. Neurol.* **57,** 535–541 (2005).
13 Mizuta, I., Satake, W., Nakabayashi, Y., Ito, C., Suzuki, S., Momose, Y. *et al.* Multiple candidate gene analysis identifies α-*synuclein* as a susceptibility gene for sporadic Parkinson's disease. *Hum. Mol. Genet.* **15,** 1151–1158 (2006).
14 Satake, W., Nakabayashi, Y., Mizuta, I., Hirota, Y., Ito, C., Kubo, M. *et al.* Genome-wide association study identifies common variants at four loci as genetic risk factors for Parkinson's disease. *Nat. Genet.* **41,** 1303–1307 (2009).
15 Simon-Sanchez, J., Schulte, C., Bras, J. M., Sharma, M., Gibbs, J. R., Berg, D. *et al.* Genome-wide association study reveals genetic risk underlying Parkinson's disease. *Nat. Genet.* **41,** 1308–1312 (2009).
16 Bower, J. H., Maraganore, D. M., McDonnell, S. K. & Rocca, W. A. Incidence and distribution of parkinsonism in Olmsted County, Minnesota, 1976-1990. *Neurology* **52,** 1214–1220 (1999).
17 Adachi, O., Kawai, T., Takeda, K., Matsumoto, M., Tsutsui, H., Sakagami, M. *et al.* Targeted disruption of the *MyD88* gene results in loss of IL-1- and IL-18-mediated function. *Immunity* **9,** 143–150 (1998).

18 Ozaki, K., Ohnishi, Y., Iida, A., Sekine, A., Yamada, R., Tsunoda, T. *et al.* Functional SNPs in the lymphotoxin-α gene that are associated with susceptibility to myocardial infarction. *Nat. Genet.* **32,** 650–654 (2002).
19 Kuruma, H., Egawa, S., Oh-ishi, M., Kodera, Y., Satoh, M., Chen, W. *et al.* High molecular mass proteome of androgen-independent prostate cancer. *Proteomics* **5,** 1097–1112 (2005).
20 Rappsilber, J., Ishihama, Y. & Mann, M. Stop and go extraction tips for matrix-assisted laser desorption/ionization, nanoelectrospray, and LC/MS sample pretreatment in proteomics. *Anal. Chem.* **75,** 663–670 (2003).
21 Rylski, M., Amborska, R., Zybura, K., Konopacki, F. A., Wilczynski, G. M. & Kaczmarek, L. Yin Yang 1 expression in the adult rodent brain. *Neurochem. Res.* **33,** 2556–2564 (2008).
22 International Parkinson Disease Genomics Consortium, Nalls, M. A., Plagnol, V., Hernandez, D. G., Sharma, M., Sheerin, U. M. *et al.* Imputation of sequence variants for identification of genetic risks for Parkinson's disease: a meta-analysis of genome-wide association studies. *Lancet* **377,** 641–649 (2011).
23 Zabetian, C. P., Hutter, C. M., Factor, S. A., Nutt, J. G., Higgins, D. S., Griffith, A. *et al.* Association analysis of *MAPT* H1 haplotype and subhaplotypes in Parkinson's disease. *Ann. Neurol.* **62,** 137–144 (2007).
24 Stefansson, H., Helgason, A., Thorleifsson, G., Steinthorsdottir, V., Masson, G., Barnard, J. *et al.* A common inversion under selection in Europeans. *Nat. Genet.* **37,** 129–137 (2005).
25 Shi, Y., Lee, J. S. & Galvin, K. M. Everything you have ever wanted to know about Yin Yang 1..... *Biochim. Biophys. Acta* **1332,** F49–F66 (1997).
26 Gordon, S., Akopyan, G., Garban, H. & Bonavida, B. Transcription factor YY1: structure, function, and therapeutic implications in cancer biology. *Oncogene* **25,** 1125–1142 (2006).
27 Shrivastava, A. & Calame, K. An analysis of genes regulated by the multi-functional transcriptional regulator Yin Yang-1. *Nucleic Acids Res.* **22,** 5151–5155 (1994).
28 Fuchs, J., Tichopad, A., Golub, Y., Munz, M., Schweitzer, K. J., Wolf, B. *et al.* Genetic variability in the *SNCA* gene influences α-synuclein levels in the blood and brain. *FASEB J.* **22,** 1327–1334 (2008).
29 Linnertz, C., Saucier, L., Ge, D., Cronin, K. D., Burke, J. R., Browndyke, J. N. *et al.* Genetic regulation of α-synuclein mRNA expression in various human brain tissues. *PLoS One* **4,** e7480 (2009).
30 Kayano, M., Takigawa, I., Shiga, M., Tsuda, K. & Mamitsuka, H. Efficiently finding genome-wide three-way gene interactions from transcript- and genotype-data. *Bioinformatics* **25,** 2735–2743 (2009).
31 Wang, Y., Joseph, S. J., Liu, X., Kelley, M. & Rekaya, R. SNPxGE^2: a database for human SNP-coexpression associations. *Bioinformatics* **28,** 403–410 (2012).
32 Costa, F. F. Non-coding RNAs: meet thy masters. *Bioessays* **32,** 599–608 (2010).
33 Faghihi, M. A., Modarresi, F., Khalil, A. M., Wood, D. E., Sahagan, B. G., Morgan, T. E. *et al.* Expression of a noncoding RNA is elevated in Alzheimer's disease and drives rapid feed-forward regulation of β-secretase. *Nat. Med.* **14,** 723–730 (2008).
34 Modarresi, F., Faghihi, M. A., Lopez-Toledano, M. A., Fatemi, R. P., Magistri, M., Brothers, S. P. *et al.* Inhibition of natural antisense transcripts in vivo results in gene-specific transcriptional upregulation. *Nat. Biotechnol.* **30,** 453–459 (2012).
35 Chandra, S., Gallardo, G., Fernández-Chacón, R., Schlüter, O. M. & Südhof, T. C. α-synuclein cooperates with CSPα in preventing neurodegeneration. *Cell* **123,** 383–396 (2005).
36 Musgrove, R. E. J., King, A. E. & Dickson, T. C. Neuroprotective upregulation of endogeneous alpha-synuclein precedes ubiquitination in cultured dopaminergic neurons. *Neurotox. Res.* **19,** 592–602 (2011).

Supplementary Information accompanies the paper on Journal of Human Genetics website (http://www.nature.com/jhg)

J Neurol (2013) 260:1664–1666
DOI 10.1007/s00415-013-6916-0

LETTER TO THE EDITORS

A novel mutation in the C2 domain of protein kinase C gamma associated with spinocerebellar ataxia type 14

Takehiro Ueda · Tsuneyoshi Seki · Kimitaka Katanazaka · Kenji Sekiguchi · Kazuhiro Kobayashi · Fumio Kanda · Tatsushi Toda

Received: 30 January 2013 / Revised: 3 April 2013 / Accepted: 4 April 2013 / Published online: 21 April 2013

Dear Sirs,

Spinocerebellar ataxia type 14 (SCA14; Online Mendelian Inheritance in Man, OMIM #605361) is an autosomal dominant neurodegenerative disorder characterized by mild and slowly progressive cerebellar ataxia. Additional symptoms, including myoclonus, spasticity, dystonia, disturbance of deep sensation, and cognitive impairment, are observed in some patients [1, 2]. The SCA14 is caused by mutations in the *protein kinase C gamma* (*PRKCG*) gene (OMIM *176980), which encodes protein kinase C gamma (PKCγ). *PRKCG* contains 18 exons, and the PKCγ protein is composed of regulatory C1 and C2 domains and catalytic C3 and C4 domains. Most *PRKCG* mutations described till this date lie in the C1 domain [3, 4], while no mutations have been found in the C2 domain so far. Here we describe, for the first time, a mutation in the C2 domain in a patient with a typical SCA14 phenotype.

A 58-year-old Japanese woman visited our hospital with gait disturbance and lisping, the latter being noticed by her husband. At the age of 40, she frequently experienced unsteadiness. At the age of 55, she visited a clinic after experiencing a fall, and brain imaging revealed cerebellar atrophy. Her father suffered from gait disturbance and dysphagia in his late 70s, and her father's brother (the patient's uncle) and his nephew (the patient's cousin) had an unsteady gait. This family history indicated autosomal dominant inheritance (Fig. 1a).

T. Ueda (✉) · T. Seki · K. Katanazaka · K. Sekiguchi · K. Kobayashi · F. Kanda · T. Toda
Division of Neurology/Molecular Brain Science, Kobe University Graduate School of Medicine, 7-5-1, Kusunoki-chou, Chuo-ku, Kobe 650-0017, Japan
e-mail: taueda@med.kobe-u.ac.jp

Neurological examination revealed cerebellar ataxia, including slurred speech, saccadic eye movement, and limb and truncal ataxia. Although there was a mild decrease in the deep sensations in her lower limbs, her gait disturbance was mostly consistent with ataxic gait. At her first visit to our institution, she had a score of 27/100 on the International Cooperative Ataxia Rating Scale. Blood, respiratory function, and cerebrospinal fluid tests yielded no remarkable findings. Brain magnetic resonance imaging demonstrated cerebellar atrophy, particularly in the upper part (Fig. 1b), and *N*-isopropyl-*p*-[123I]-iodoamphetamine single-photon emission computed tomography revealed decreased blood flow only in the upper cerebellum. She had no autonomic failure or cognitive dysfunction. Clinically, her symptoms corresponded with typical SCA14 features.

While she had a family history of autosomal dominant inheritance, genetic testing for SCA types 1, 2, 3, 6, 7, 8, and 31 and dentatorubral–pallidoluysian atrophy, genes relatively frequent in Japan, did not show the presence of abnormal alleles. Next, to test for mutations in *PRKCG*, we performed genomic PCR followed by a direct sequencing analysis. This revealed the presence of the single-base substitution c.518T>G in exon five involving amino acid change p.Ile173Ser (Fig. 1c). This substitution has not been reported, either as a single-nucleotide polymorphism or as a mutation. The amino acid p.Ile173 residue is conserved among PRKCG proteins from mammals and zebrafish (Fig. 1d). To ascertain whether this was a disease-associated mutation, we first performed direct sequencing of this region in 200 Japanese healthy controls and found that none of them carried this alternative allele. Next, we employed three computer algorithms to predict the effect of this novel mutation: Sorting Intolerant From Tolerant (SIFT, http://sift.bii.a-star.edu.sg/), Polymorphism Phenotyping v2

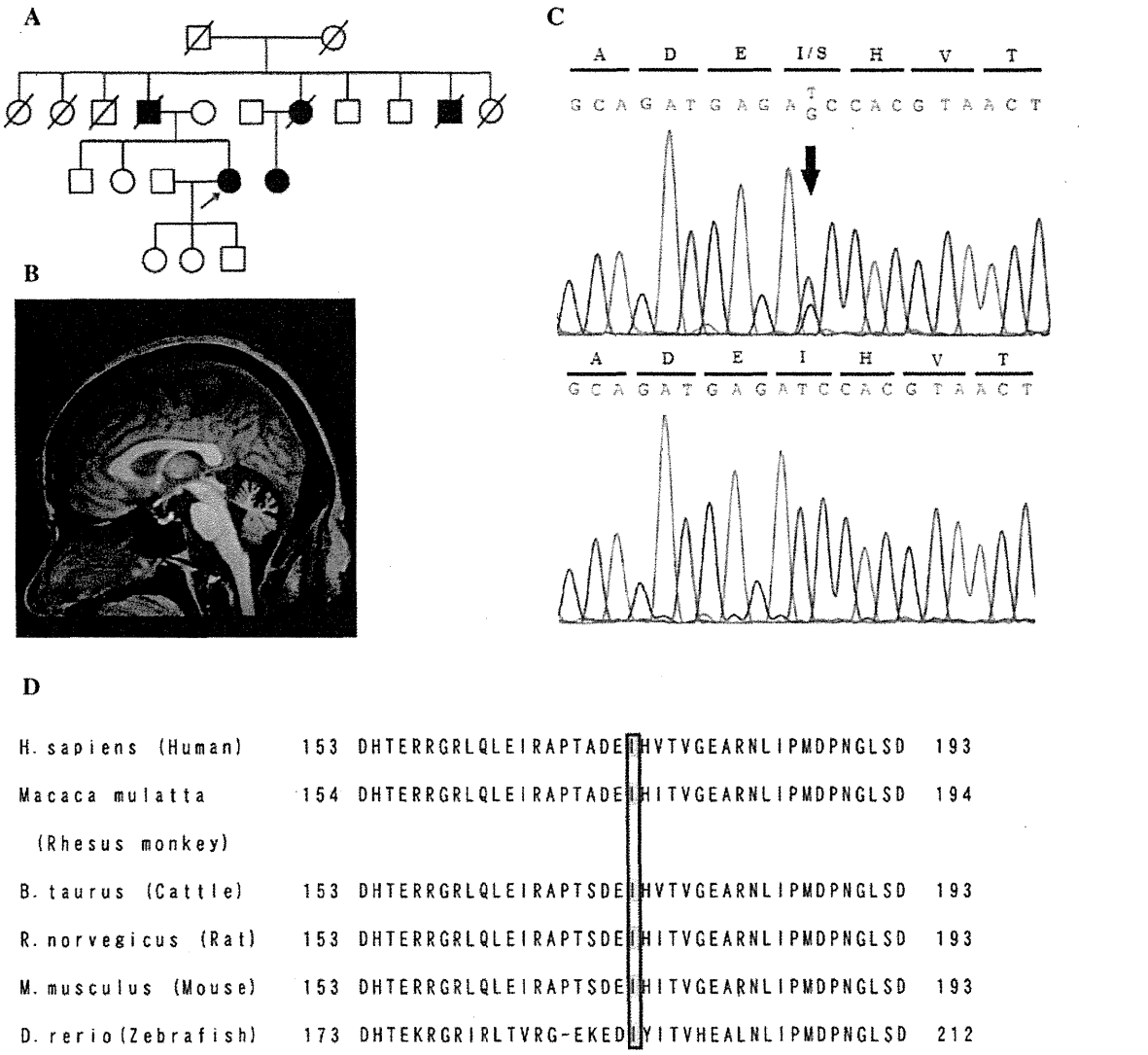

Fig. 1 **a** Family tree of the presented case. Autosomal dominant inheritance is indicated. **b** Sagittal view of T1 weighted magnetic resonance imaging in this patient shows marked atrophy in the upper cerebellum. **c** Sequencing analysis of exon five in PRKCG. The patient (*upper column*) has heterozygous c.518T>G substitution (p.Ile173Ser) whereas normal control (*lower column*) has no mutation. **d** The amino acid p.Ile173 residue is conserved among PRKCG proteins from mammals and zebrafish

(PolyPhen-2, http://genetics.bwh.harvard.edu/pph2/) and MutationTaster (http://www.mutationtaster.org). These programs predicted p.Ile173Ser to be 'damaging', 'possibly damaging' and 'disease causing', respectively. This novel mutation was located in the C2 domain of the PKCγ protein, which comprises amino acids 172–275 [5].

Since the first description of SCA14-causative mutations in *PRKCG* in 2003 [5], over 20 mutations have been reported. As mentioned above, most mutations lie in the C1 domain, which contributes to the localization of the protein. In contrast, no mutations had been found in the C2 domain, which functions as a Ca^{2+} sensor. Both these domains play an important role in the maintenance of Ca^{2+} homeostasis [6]. This novel mutation (p.Ile173Ser) may change protein function by altering its chemical properties from hydrophobic to hydrophilic. It is expected that this novel mutation will facilitate our understanding of PKCγ function and SCA14 pathogenesis.

Acknowledgments We thank the members of our laboratory, especially Ms. Ando Y., for genetic testing.

Conflicts of interest All authors report no conflicts of interest.

Ethical standard This study has been approved by the appropriate ethics committee and has, therefore, been performed in accordance with the ethical standards laid down in the 1964 Declaration of Helsinki.

References

1. Durr A (2010) Autosomal dominant cerebellar ataxias: polyglutamine expansions and beyond. Lancet Neurol 9:885–894
2. Klebe S, Durr A, Rentschler A, Hahn-Barma V, Abele M, Bouslam N, Schöls L, Jedynak P, Forlani S, Denis E, Dussert C, Agid Y, Bauer P, Globas C, Wüllner U, Brice A, Riess O, Stevanin G (2005) New mutations in protein kinase C gamma associated with spinocerebellar ataxia type 14. Ann Neurol 58:720–729
3. Dalski A, Mitulla B, Bürk K, Schattenfroh C, Schwinger E, Zühlke C (2006) Mutation of the highly conserved cysteine residue 131 of the SCA14 associated PRKCG gene in a family with slow progressive cerebellar ataxia. J Neurol 253:1111–1112
4. Koht J, Stevanin G, Durr A, Mundwiller E, Brice A, Tallaksen CM (2012) SCA14 in Norway, two families with autosomal dominant cerebellar ataxia and a novel mutation in the PRKCG gene. Acta Neurol Scand 125:116–122
5. Chen DH, Brkanac Z, Verlinde CL, Tan XJ, Bylenok L, Nochlin D, Matsushita M, Lipe H, Wolff J, Fernandez M, Cimino PJ, Bird TD, Raskind WH (2003) Missense mutations in the regulatory domain of PKC gamma: a new mechanism for dominant nonepisodic cerebellar ataxia. Am J Hum Genet 72:839–849
6. Adachi N, Kobayashi T, Takahashi H, Kawasaki T, Shirai Y, Ueyama T, Matsuda T, Seki T, Sakai N, Saito N (2008) Enzymological analysis of mutant protein kinase Cgamma causing spinocerebellar ataxia type 14 and dysfunction in Ca^{2+} homeostasis. J Biol Chem 283:19854–19863

Human Molecular Genetics, 2013, Vol. 22, No. 15 **3003–3015**
doi:10.1093/hmg/ddt157
Advance Access published on April 4, 2013

Impaired viability of muscle precursor cells in muscular dystrophy with glycosylation defects and amelioration of its severe phenotype by limited gene expression

Motoi Kanagawa[1], Chih-Chieh Yu[1,†], Chiyomi Ito[1,†], So-ichiro Fukada[2], Masako Hozoji-Inada[1], Tomoko Chiyo[3], Atsushi Kuga[1], Megumi Matsuo[1], Kanoko Sato[1], Masahiko Yamaguchi[2], Takahito Ito[2], Yoshihisa Ohtsuka[1], Yuki Katanosaka[4], Yuko Miyagoe-Suzuki[3], Keiji Naruse[4], Kazuhiro Kobayashi[1], Takashi Okada[3], Shin'ichi Takeda[3] and Tatsushi Toda[1,*]

[1]Division of Neurology/Molecular Brain Science, Kobe University Graduate School of Medicine, Kobe 650-0017, Japan, [2]Laboratory of Molecular and Cellular Physiology, Graduate School of Pharmaceutical Sciences, Osaka University, Suita 565-0871, Japan, [3]Department of Molecular Therapy, National Institute of Neuroscience, National Center of Neurology and Psychiatry, Kodaira 187-8502, Japan and [4]Department of Cardiovascular Physiology, Graduate School of Medicine, Dentistry and Pharmaceutical Sciences, Okayama University, Okayama 700-8558, Japan

Received January 7, 2013; Revised March 3, 2013; Accepted April 2, 2013

A group of muscular dystrophies, dystroglycanopathy is caused by abnormalities in post-translational modifications of dystroglycan (DG). To understand better the pathophysiological roles of DG modification and to establish effective clinical treatment for dystroglycanopathy, we here generated two distinct conditional knock-out (cKO) mice for *fukutin*, the first dystroglycanopathy gene identified for Fukuyama congenital muscular dystrophy. The first dystroglycanopathy model—myofiber-selective fukutin-cKO [muscle creatine kinase (MCK)-fukutin-cKO] mice—showed mild muscular dystrophy. Forced exercise experiments in presymptomatic MCK-fukutin-cKO mice revealed that myofiber membrane fragility triggered disease manifestation. The second dystroglycanopathy model—muscle precursor cell (MPC)-selective cKO (Myf5-fukutin-cKO) mice—exhibited more severe phenotypes of muscular dystrophy. Using an isolated MPC culture system, we demonstrated, for the first time, that defects in the fukutin-dependent modification of DG lead to impairment of MPC proliferation, differentiation and muscle regeneration. These results suggest that impaired MPC viability contributes to the pathology of dystroglycanopathy. Since our data suggested that frequent cycles of myofiber degeneration/regeneration accelerate substantial and/or functional loss of MPC, we expected that protection from disease-triggering myofiber degeneration provides therapeutic effects even in mouse models with MPC defects; therefore, we restored fukutin expression in myofibers. Adeno-associated virus (AAV)-mediated rescue of fukutin expression that was limited in myofibers successfully ameliorated the severe pathology even after disease progression. In addition, compared with other gene therapy studies, considerably low AAV titers were associated with therapeutic effects. Together, our findings indicated that fukutin-deficient dystroglycanopathy is a regeneration-defective disorder, and gene therapy is a feasible treatment for the wide range of dystroglycanopathy even after disease progression.

*To whom correspondence should be addressed at: 7-5-1 Kusunoki-chou Chuo-ku, Kobe 650-0017, Japan. Tel: +81 783826287; Fax: +81 783826288; Email: toda@med.kobe-u.ac.jp
†These authors contributed equally to this work.

INTRODUCTION

Dystroglycanopathy includes Walker–Warburg syndrome, muscle–eye–brain disease, Fukuyama congenital muscular dystrophy (FCMD) and several forms of congenital and limb–girdle muscular dystrophies (1). Dystroglycanopathy is indicated by a wide variety of clinical symptoms; the most severe end of the clinical spectrum is characterized by congenital muscular dystrophy with severe structural brain and eye abnormalities, whereas the mildest end presents in adult life with limb–girdle muscular dystrophy without brain or eye involvement (1). FCMD is the first dystroglycanopathy to be reported (2,3), and it is the second most common childhood muscular dystrophy in Japan. The founder mutation, a SINE-VNTR-*Alu* retrotransposon insertion in the 3′ noncoding region of *fukutin*, causes abnormal splicing that leads to the production of non-functional proteins in FCMD (4,5). FCMD is characterized by severe congenital muscular dystrophy, abnormal neuronal migration associated with mental retardation and epilepsy and, frequently, eye abnormalities. It often results in early death before the age of 20 (6). Several point mutations in *fukutin* have also been reported to be associated with dystroglycanopathy in Japan and other countries (7,8).

More than 10 genes [protein *O*-mannosyltransferase 1 (*POMT1*), protein *O*-mannosyltransferase 2 (*POMT2*), protein *O*-linked mannose β-1,2-*N*-acetylglucosaminyltransferase 1 (*POMGNT1*), *fukutin*, fukutin-related protein (*FKRP*), *LARGE*, dolichol-phosphate-mannose synthase (*DPM2* and *DPM3*), isoprenoid synthase domain containing (*ISPD*) gene, glycosyltransferase-like domain containing 2 (*GTDC2*) gene and β-1,3-*N*-acetylglucosaminyltransferase 1 (*B3GNT1*)], implicated in dystroglycanopathies, have been shown or expected to be involved in the glycosylation pathway of α-dystroglycan (α-DG) (1,9,10). POMGnT1 and the POMT1/2 complex possess glycosyltransferase activities and can directly synthesize *O*-mannosyl sugar chains on α-DG (11,12). Fukutin, FKRP and LARGE are involved in a novel phosphodiester-linked modification, namely, a post-phosphoryl modification, of *O*-mannose on α-DG (13,14). Recently, it has been shown that LARGE can act as a bifunctional glycosyltransferase with both xylosyltransferase and glucuronyltransferase activities (15). The DG gene *DAG1* encodes both α- and β-DG, which is post-translationally cleaved into the two subunits (16). α-DG is a highly glycosylated protein and serves as the receptor subunit for extracellular proteins such as laminins, perlecan, agrin, neurexin and pikachurin (9,17). *O*-mannosyl glycosylation and the post-phosphoryl modification are required for the ligand-binding activities of α-DG (3,13). Hypoglycosylation and reduced ligand-binding activity of α-DG are common characteristics of dystroglycanopathy. α-DG is anchored to the plasma membrane through non-covalent interactions with the transmembrane subunit β-DG. β-DG intracellularly interacts with dystrophin, whose mutations lead to Duchenne/Becker muscular dystrophy, and dystrophin, in turn, binds to actin filaments. This molecular linkage, created by laminin-DG-dystrophin-actin filaments, is thought to provide mechanical stability to the plasma membrane of the muscle fiber; thus, disruption of this linkage is considered a key pathological event in several forms of muscular dystrophy. In FCMD skeletal muscles, in addition to dystrophic muscular changes, there are certain characteristics such as intensive connective tissue infiltration and the presence of predominant small-sized fibers from the early infantile stage (6). Furthermore, aberrant neuromuscular junctions and delayed muscle fiber maturation have been implicated in the pathology of FCMD (18). FCMD also shows central nervous system involvement. Together, these data suggest that more complex and unknown physiological roles of α-DG modification underlie the skeletal muscle pathology of dystroglycanopathy.

Recent studies have identified new genes associated with dystroglycanopathy (19–21), and an increasing number of patients are being diagnosed with dystroglycanopathy worldwide. However, the pathogenesis of this condition is not fully understood, and no effective clinical treatment has been established. To understand the pathogenesis and establish a therapeutic strategy for dystroglycanopathy, we developed two distinct *fukutin* conditional knock-out (cKO) mice as models for dystroglycanopathy. In our study, investigation of presymptomatic fukutin-deficient mice provided direct evidence that fragility of the myofiber membrane triggers the pathogenesis of dystroglycanopathy. We also used an isolated muscle precursor cell (MPC) culture system to demonstrate, for the first time, that defects in the fukutin-dependent modification of DG lead to impairment of MPC proliferation, differentiation and muscle regeneration. We predicted that protection from disease-triggering myofiber degeneration would prevent substantial and/or functional loss of MPC, thereby providing therapeutic effects. Indeed, we demonstrate that restoration of fukutin expression in myofibers successfully ameliorates the severe pathology even after disease progression. These results indicate that gene therapy is a feasible treatment for dystroglycanopathy.

RESULTS

Generation and characterization of myofiber-selective fukutin cKO mice

To generate *fukutin*-cKO mice, flox fukutin mice (*fukutin*$^{lox/lox}$) were crossed with muscle creatine kinase (MCK)-Cre mice (22) or Myf5-Cre mice (23), which express the *Cre* gene with the help of the MCK promoter or Myf5 promoter, respectively (Supplementary Material, Fig. S1). The MCK promoter is active in differentiating and differentiated muscle cells (24), and MCK expression reaches maximum levels at post-natal day 10 and remains constantly high throughout life (25). First, we analyzed the MCK-fukutin-cKO mice at different time points. In the skeletal muscles of these mice, we confirmed dramatic reduction in the fukutin protein after the age of 4 weeks (Fig. 1A). Abnormal modification of α-DG is indicated by decreased molecular weight, loss of immunoreactivity against the monoclonal IIH6 antibody, which recognizes properly glycosylated α-DG (3), and decreased laminin-binding activity. Abnormally modified α-DG was predominant in MCK-fukutin-cKO mice aged >8 weeks (Fig. 1A). Loss of the post-phosphoryl modification was further confirmed by subjecting the protein to treatment with cold aqueous hydrofluoric (HF) acid, which cleaves phosphoester linkages, and to inorganic metal-affinity chromatography (IMAC), which captures monoester-linked phosphorylated compounds

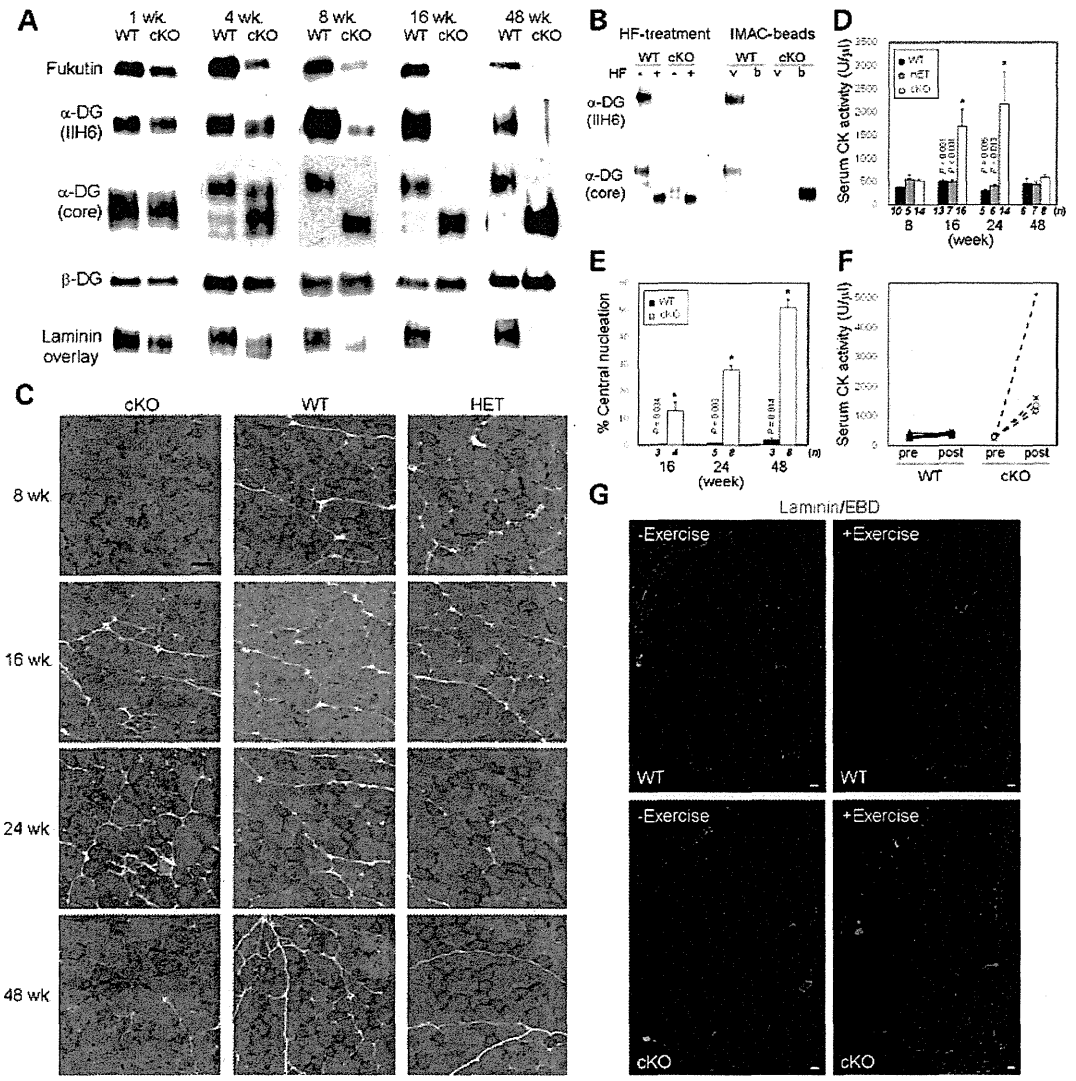

Figure 1. Pathological characterization of MCK-fukutin-cKO mice. **(A)** Western blot analysis of fukutin protein expression and α-DG modification in MCK-fukutin-cKO (cKO) and litter control WT skeletal muscles at different ages (1, 4, 8, 16 and 48 weeks). β-DG was used as a loading control. Laminin-binding activity of α-DG was examined by the laminin overlay assay. **(B)** Post-phosphoryl modification of α-DG from MCK-fukutin-cKO and control WT skeletal muscles. The absence of the post-phosphoryl modification was confirmed by HF treatment and IMAC-bead-binding assay. The void (v) and bound (b) fractions of the IMAC beads were analyzed by western blotting. **(C)** H&E staining of tibialis anterior muscles. Bar □50 μm. **(D)** Serum CK activity and **(E)** proportion of myofibers with centrally located nuclei. Data shown are mean ± SEM for each group (*n* is indicated in the graph). $^*P \leq 0.05$ for both cKO versus WT and cKO versus HET (D) and cKO versus WT (E) (Mann–Whitney *U* test; *P*-values are indicated in the graph). **(F)** Serum CK activity before and after forced exercise. Serum CK levels of individual mice (*n* □4 in each genotype) were measured before (pre) and after (post) exercise. **(G)** Uptake of Evans blue dye into myofibers after forced exercise. MCK-fukutin-cKO and control WT mice were subjected to forced exercise (+Exercise); subsequently, the muscle sections were stained with laminin (green) for individual fibers and merged with Evans blue dye (red). Mice not subjected to exercise were used as controls (−Exercise). Bar □200 μm.

(13,14). The molecular weight of α-DG in the skeletal muscles of control (WT) mice was dramatically reduced after HF treatment, and α-DG did not bind to IMAC beads because the phosphodiester-linked modification was intact; in contrast, α-DG in the skeletal muscles of MCK-fukutin-cKO mice showed little sensitivity to HF and bound to IMAC beads (Fig. 1B), indicating incomplete post-phosphoryl modification. Immunofluorescence staining with an antibody against an α-DG core protein showed that α-DG localized to the sarcolemma of MCK-fukutin-cKO mice as seen in normal controls (Supplementary Material, Fig. S2A), which suggests that cellular trafficking of α-DG is little affected by fukutin deficiency. These results confirmed abnormal modification of α-DG in the skeletal muscles of MCK-fukutin-cKO mice.

Hematoxylin and eosin (H&E) staining revealed that 16-week-old MCK-fukutin-cKO mice showed signs of muscular dystrophy, such as myonecrosis and central nucleation (Fig. 1C). Serum creatine kinase (CK) activity in

16-week-old MCK-fukutin-cKO mice was significantly higher than that in controls (Fig. 1D). These pathological features were not observed in 8-week-old mice (Fig. 1C and D); a possible reason may be the presence of residual α-DG with proper glycosylation (Supplementary Material, Fig. S2B). The population of myofibers with centrally located nuclei, an indication of repeated cycles of myofiber degeneration/regeneration, increased with age (Fig. 1E); however, more advanced pathology, such as infiltration of fat and connective tissues, was rarely observed even in 48-week-old MCK-fukutin-cKO mice (Fig. 1C).

It has been widely believed that functional and/or substantial loss of DG-containing protein complexes (i.e. the dystrophin–glycoprotein complex) leads to disease-causing membrane fragility. This concept is based on results of forced exercise experiments in animals with muscular dystrophy, which led to increases in the serum CK levels and uptake of membrane-impermeable Evans blue dye by myofibers (26,27). However, these experiments were conducted in diseased animals; therefore, it remains unclear whether membrane fragility triggers disease-causing phenotype. Therefore, we subjected 10-week-old MCK-fukutin-cKO mice, which showed abnormal α-DG modification but no pathology (Supplementary Material, Fig. S2C), to forced exercise. After forced exercise, serum CK levels were dramatically increased in the MCK-fukutin-cKO mice but not in the control mice (Fig. 1F). Myofibers with membrane-impermeable Evans blue dye uptake were also observed only in the exercise-administered MCK-fukutin-cKO mice (Fig. 1G). These data indicate that the plasma membrane of the muscle cells becomes weak before disease onset, providing proof-of-principle that membrane fragility triggers disease manifestation.

Characterization of MPC-selective fukutin cKO mice

Loss of fukutin in differentiated myofibers results in only mild and slow-progressing disease-causing phenotypes. We hypothesized that fukutin-dependent modification also plays a role in MPCs that are not targeted by MCK-Cre-mediated recombination. Therefore, we generated cKO mice lacking fukutin in MPCs by crossing flox fukutin mice with Myf5-Cre knock-in mice (23) expressing Cre recombinase under the control of the endogenous Myf5 promoter (Myf5-fukutin-cKO mice; Supplementary Material, Fig. S1). It has been reported that the Myf5-Cre allele recapitulates the expression pattern of the endogenous Myf5 gene and is uniformly expressed in all proliferating myoblasts (23). The Myf5-fukutin-cKO mice grossly show little difference compared with the litter controls until ~2 weeks of age; thereafter, increase in body weight was significantly retarded (Fig. 2A). Most Myf5-fukutin-cKO mice died by 6 months (Fig. 2B). Reduction in fukutin protein expression and abnormal modification were confirmed by immunofluorescence, western blotting, HF treatment and IMAC-bead assay (Fig. 2C and D). As is the case of MCK-fukutin-cKO, α-DG in Myf5-fukutin-cKO localizes to the sarcolemma (Supplementary Material, Fig. S2D). H&E staining revealed progressive pathological changes in Myf5-fukutin-cKO skeletal muscles (Fig. 2E). At 2 weeks, myonecrotic fibers were sparse (Supplementary Material, Fig. S2E), and at 4 weeks, in addition to myonecrotic fibers, myofibers with centrally located nuclei were observed (Fig. 2E). Serum CK levels and the proportion of the myofibers with centrally located nuclei were significantly higher in Myf5-fukutin-cKO mice than in the controls at 4, 8 and 16 weeks (Fig. 2F and G). Sixteen-week-old Myf5-fukutin-cKO mice showed more advanced pathological changes, such as fiber size variation and fibrosis (Fig. 2E). A few specimens showed milder phenotypic changes accompanied by increases in the normally glycosylated α-DG population (Supplementary Material, Fig. S2F). Overall, different phenotypes of the MCK-fukutin-cKO and Myf5-fukutin-cKO mice suggested a pathophysiological role of fukutin-dependent modification in MPCs.

Impaired viability of MPCs in Myf5-fukutin-cKO mice

To determine the impact of fukutin deficiency on MPC activity, we isolated SM/C-2.6(+) satellite cells from young (slightly affected) and adult (diseased) Myf5-fukutin-cKO muscles and then cultured them as MPCs (i.e. myoblasts) (28). The number of isolated SM/C-2.6(+) cells tended to be less in young fukutin-deficient muscles and was significantly reduced in adults compared with the litter controls (Fig. 3A). The proliferation activity of the isolated MPCs was slightly but significantly decreased in young and severely reduced in adult Myf5-fukutin-cKO muscles (Fig. 3B). The differentiation activity of fukutin-deficient myoblasts was significantly lower than that of the control mice (Fig. 3C). Quantification of the Pax7 immunofluorescence signal, a satellite cell marker, on skeletal muscle sections also suggested decreases in the number of satellite cells in adult Myf5-fukutin-cKO mice compared with control mice (Supplementary Material, Fig. S3A). We also examined the population of activated satellite cells by Pax7/MyoD double staining on the skeletal muscle sections from Myf5-fukutin-cKO mice. The results suggested that the number of active satellite cells was reduced in 16-week-old Myf5-fukutin-cKO mice compared with that in 8-week-old Myf5-fukutin-cKO mice (Supplementary Material, Fig. S3B). These data suggest that in addition to decreases in the number of satellite cells, the activation state of satellite cells is impaired in Myf5-cKO mice as the disease progresses.

We next examined *in vivo* regeneration capability of the Myf5-fuktuin-cKO muscles after cardiotoxin (CTX)-induced muscle degeneration. After 14 days of the CTX challenge in adult mice (~3 months old), we observed that the proportion of small myofibers was strikingly higher in Myf5-fukutin-cKO mice than in the controls (Fig. 3D and E). In some cases, the CTX-injected Myf5-fukutin-cKO muscles showed severe atrophic changes compared with the contralateral saline-injected ones (Supplementary Material, Fig. S3C). In younger (~4 weeks old) Myf5-fukutin-cKO mice, after 14 days of the CTX challenge, no obvious histological difference was noted compared with the controls (Supplementary Material, Fig. S3D); however, after 5 days of the CTX challenge, the proportion of smaller regenerating fibers (that are embryonic myosin-positive) was higher in Myf5-fukutin-cKO muscles than in the controls (Supplementary Material, Fig. S3E and F). These minor impairments in the regeneration of younger Myf5-fukutin-cKO skeletal muscles are consistent with the *in vitro* results. Overall, our data showed that fukutin-dependent

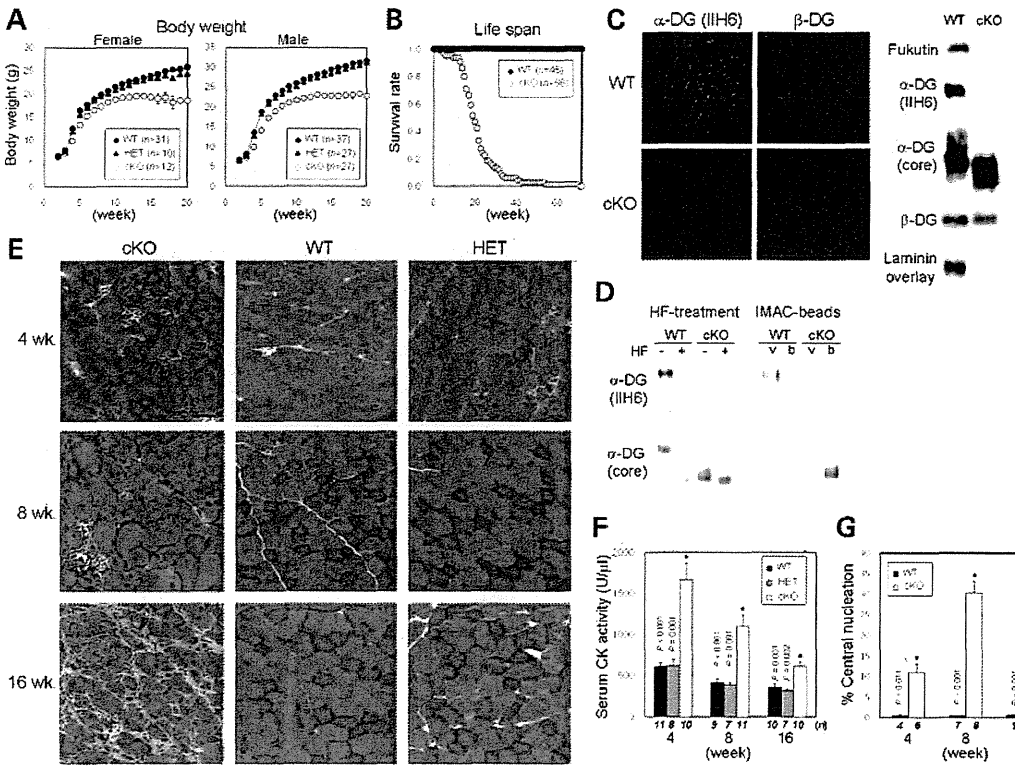

Figure 2. Pathological characterization of Myf5-fukutin-cKO mice. (**A**) Temporal changes in body weight. Data shown are mean ± SEM for each group (*n* is indicated in the graph). (**B**) Survival curve of Myf5-fukutin cKO mice. (**C**) Immunofluorescence and western blot analyses of fukutin expression and α-DG modification. Skeletal muscles of new born and 1-week-old Myf5-fukutin-cKO and control WT mice were used for immunofluorescence and western blotting, respectively. β-DG was used as a control. Laminin-binding activity of α-DG was examined by the laminin overlay assay. (**D**) Post-phosphoryl modification of α-DG from Myf5-fukutin-cKO and control WT skeletal muscles. The absence of post-phosphoryl modification was tested by HF treatment and IMAC-bead-binding assay. The void (v) and bound (b) fractions of the IMAC beads were analyzed by western blotting. (**E**) H&E staining of tibialis anterior muscles. Bar □50 μm. (**F**) Serum creatin kinase activity and (**G**) proportion of myofibers with centrally located nuclei. Data shown are mean ± SEM for each group (*n* is indicated in the graph). $^*P \leq 0.05$ for both cKO versus WT and cKO versus HET (F) and cKO versus WT (G) (Mann–Whitney *U* test; *P*-values are indicated in the graph).

modification plays important roles in maintaining MPC viability, and consequently, muscle regeneration capability, suggesting that these defects may contribute to the severe phenotype of dystroglycanopathy.

Amelioration of the severe pathology by limited fukutin rescue in myofibers

Our pathological analysis of the two distinct fukutin-cKO mice suggested that membrane fragility triggers disease manifestation and that impaired MPC viability is related to disease progression and severity of dystroglycanopathy. These findings indicate that a therapeutic strategy must involve prevention of myofiber membrane weakness and/or rescue of substantial loss and dysfunction of MPCs. In addition, dystroglycanopathy is usually diagnosed after disease manifestation, and thus, treatments should be effective even after disease progression. Since our data suggested that frequent cycles of myofiber degeneration/regeneration accelerate substantial and/or functional loss of MPC, we expected that protection from disease-triggering myofiber degeneration provides therapeutic effects even in mouse models with MPC defects. In this study, to prevent disease-causing myofiber degeneration, we examined whether rescue of fukutin expression that is limited in myofibers is therapeutically beneficial in Myf5-fukutin-cKO mice. Therefore, we constructed recombinant AAV9 (AAV, adeno-associated virus) vectors containing the mouse *fukutin* cDNA under the MCK promoter (AAV9-MCK-*fukutin*).

We first administered intramuscular injections of AAV9-MCK-*fukutin* to 1-week-old (i.e. before disease manifestation) or 8-week-old (i.e. after disease manifestation) Myf5-fukutin-cKO mice; then, we examined the therapeutic effects after 2 months. In both cases, fukutin protein expression was higher in the AAV-injected Myf5-fukutin-cKO muscles than in the control WT muscles (endogenous fukutin protein in muscle lysates is below detectable levels) (Fig. 4A and E). IIH6-positive α-DG was restored, indicating functional rescue of *fukutin* gene expression even in adult cases (Fig. 4A, B, E and F). Histological and quantitative analyses showed that gene transfer at 1 week prevented disease manifestation (Fig. 4C and D). When gene transfer was challenged in 8-week-old mice, H&E staining showed milder phenotype in AAV-treated Myf5-fukutin-cKO muscles than

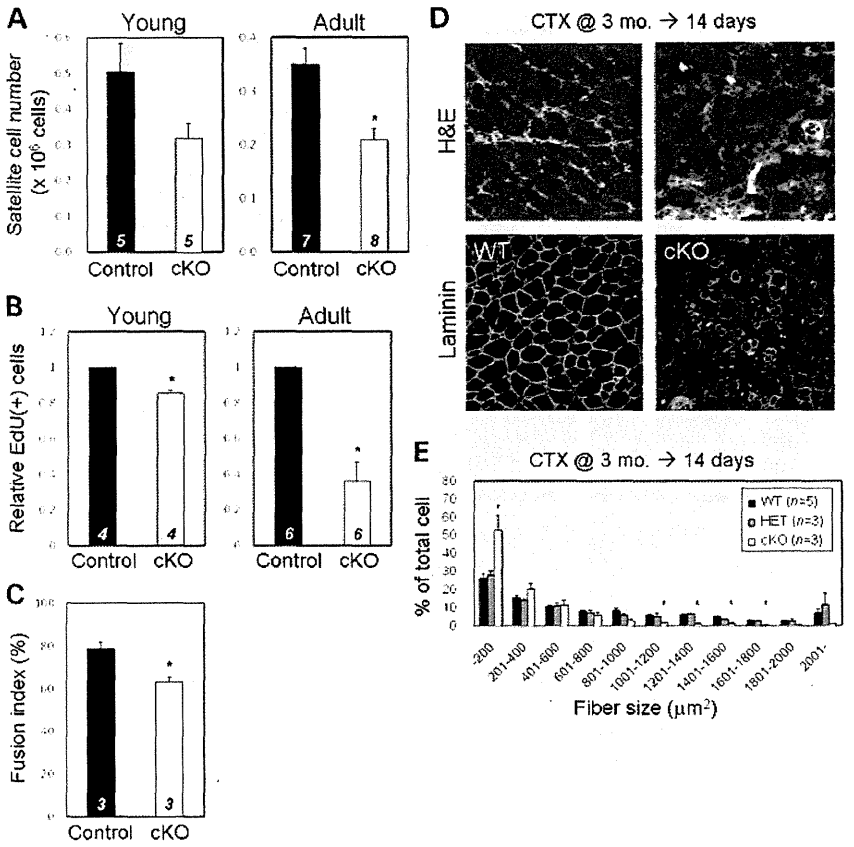

Figure 3. Impaired MPC activities and muscle regeneration in Myf5-fukutin-cKO mice. (**A**) The number of isolated satellite cells from young (2 weeks old) and adult (4 months old) Myf5-fukutin-cKO mice. P □0.117 for young, and P □0.005 for adult (Mann–Whitney U test). (**B**) Proliferation activity of the isolated MPCs. MPCs from young or adult Myf5-fukutin-cKO muscles were cultured for 2 days, and 5-ethynyl-2′-deoxyuridine-positive (EdU+) cells were counted. P □0.014 for young, and P □0.002 for adult (Mann–Whitney U test). (**C**) Differentiation activity of the isolated MPCs. MPCs from young Myf5-fukutin-cKO muscles were cultured in growth media for 2 days and then in differentiation media for 2 days. The cells were fixed, and multinucleated myotubes were counted. P □0.05 (Mann–Whitney U test). For (A)–(C), data shown are mean ± SEM for each group (n is indicated in the graph). $^*P \leq 0.05$ compared with litter controls (Mann–Whitney U test). (**D**) Regeneration after CTX-induced muscle degeneration. CTX was injected into the tibialis anterior muscles of 3-month-old Myf5-fukutin-cKO and control mice (WT and HET). After 14 days, the muscle sections were analyzed by H&E staining and immunofluorescence staining with laminin. (**E**) Quantitative analysis for myofiber size variation after the CTX challenge. Data shown are mean ± SEM for each group (n is indicated in the graph). $^*P \leq 0.05$ for both cKO versus WT and cKO versus HET (Mann–Whitney U test).

in non-treated ones (Fig. 4G). Quantitatively, connective tissue infiltration and prevalence of small fibers were significantly reduced (Fig. 4H and I), whereas a substantial number of myofibers with central nucleation was still present after the gene transfer (Fig. 4J).

Next, we examined systemic delivery of the *fukutin* gene via tail vein injection into 4-week-old Myf5-fukutin-cKO mice with early-stage muscular dystrophy, primarily because diagnosis occurs during this stage in humans. After 2 months of the injection, we confirmed fukutin protein expression and recovery of α-DG modification in the treated Myf5-fukutin-cKO mice (Fig. 5A and B). After gene transfer, body and muscle weight were restored (Fig. 5C and D), and grip strength was dramatically improved, indicating recovery of muscle physiological function (Fig. 5E). H&E staining (Fig. 5F) and quantitative analyses of connective tissue infiltration (Fig. 5G) and fiber size variation (Fig. 5H) showed amelioration of muscle pathology; however, there were still a few necrotic fibers and a substantial proportion of myofibers with centrally located nuclei (Fig. 5I). Similar therapeutic effects were also obtained in other muscles (Supplementary Material, Fig. S4). Our results show that limited recovery of fukutin expression in myofibers, even after disease progression, can successfully ameliorate the severe phenotype of Myf5-fukutin-cKO mice.

We also constructed recombinant AAV9 vectors containing the mouse *fukutin* cDNA under the CMV promoter (AAV9-CMV-*fukutin*), which is commonly used for driving the expression of transgenes in a wide range of cell types. Two months after tail-vein injection in 4-week-old Myf5-fukutin-cKO mice, we observed therapeutic effects similar to those observed in AAV9-MCK-*fukutin*-treated Myf5-fukutin-cKO mice (Supplementary Material, Fig. S5). There was no obvious difference in the efficiency for the recovery of IIH6 immunoreactivity (the proportion of IIH6-positive to laminin-positive fibers) between the cases of AAV9-MCK-*fukutin* (77.4 ± 3.8%, n □5) and AAV9-CMV-*fukutin* (74.8 ± 3.6%,

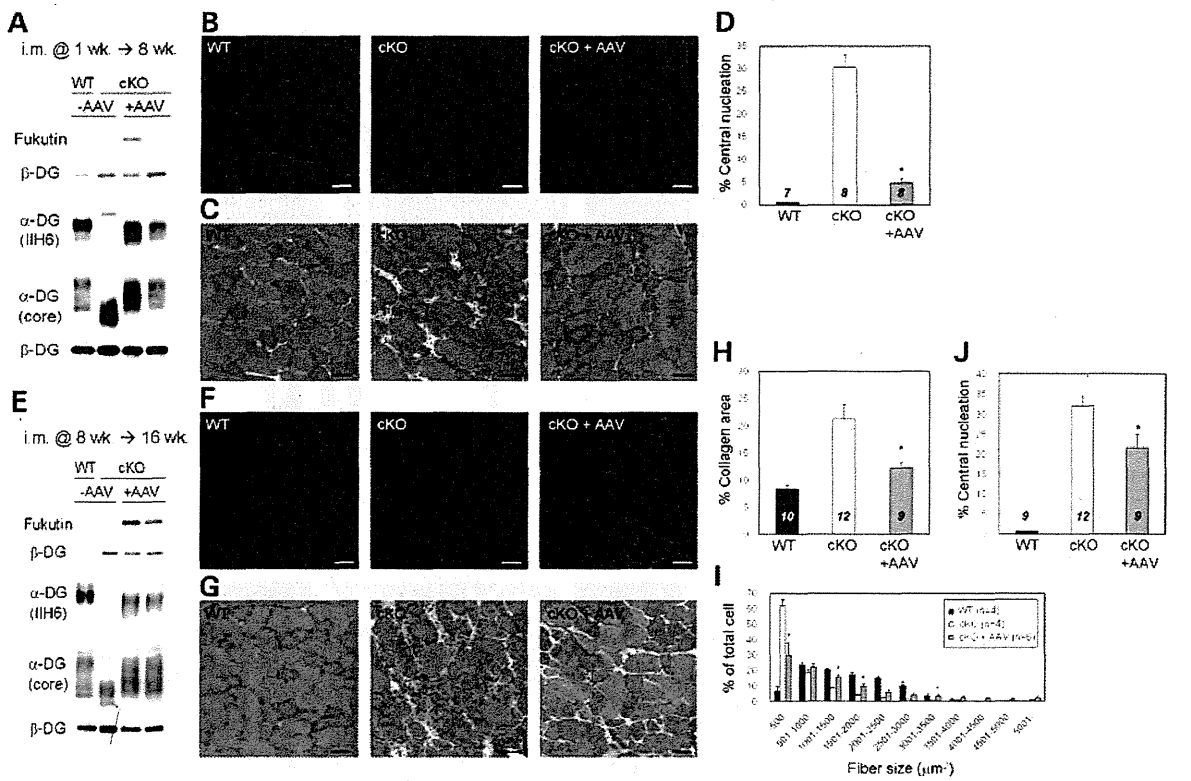

Figure 4. Gene transfer of *fukutin* via AAV9 intramuscular injection into Myf5-fukutin-cKO mice. AAV9-MCK-*fukutin* was administered to 1-week-old (**A–D**) and 8-week-old (**E–J**) Myf5-fukutin-cKO mice via intramuscular injection. Two months after the gene transfer, recovery of fukutin protein and α-DG glycosylation was confirmed by western blotting (A and E) and IIH6-immunofluorescence staining (B and F) (bar □50 μm). For fukutin protein expression and α-DG modification, total lysate and wheat germ agglutinin-enriched fractions, respectively, were subjected to western blotting. In both cases, β-DG was used as a loading control. Western blotting results for two AAV-treated mice are shown. Therapeutic effects were quantitatively evaluated in terms of the proportion of myofibers with centrally located nuclei (D; P □0.001, J; P □0.023), connective tissue infiltration (H; P □0.016) and fiber size variation (I; $^*P \leq 0.05$). Data shown are mean ± SEM for each group (n is indicated in the graph). $^*P \leq 0.05$ compared with non-treated cKO mice (Mann–Whitney U test).

n □5). In addition, the population of myofibers with centrally located nuclei was significantly improved (Supplementary Material, Fig. S5I). We also examined the effects of intraperitoneal injections of AAV9-CMV-*fukutin* in 1-week-old Myf5-fukutin-cKO mice. Two months after the injections, we observed partial recovery of α-DG glycosylation and amelioration of the pathology compared with that observed in non-treated Myf5-fukutin-cKO mice (Supplementary Material, Fig. S6A–D).

The predominant mutation in FCMD is a retrotransposon insertion (4). We previously generated a transgenic knock-in mouse model carrying this insertion (29). The knock-in Hp/− mice represent compound heterozygotes for the insertion and a nonsense *fukutin* mutation. Although Hp/− mice show abnormal glycosylation of α-DG, a small amount of intact α-DG is also present; this prevents muscular dystrophy (29). We administered intraperitoneal injections of AAV9-CMV-*fukutin* to 1-week-old Hp/− mice and examined α-DG glycosylation status after 16 and 48 weeks. We detected increased levels of fukutin expression and IIH6-positive α-DG in the AAV-treated Hp/− skeletal muscles even 48 weeks after the gene transfer (Supplementary Material, Fig. S6E). These data suggest that the transferred *fukutin* gene persists in correcting abnormal glycosylation of α-DG for a considerable length of time.

DISCUSSION

In this study, we developed and analyzed two distinct *fukutin* cKO mice to understand the pathogenesis and to establish a therapeutic strategy for dystroglycanopathy. Our data showed that MPC-selective Myf5-fukutin-cKO mice exhibited more severe phenotypes of muscular dystrophy than myofiber-selective MCK-fukutin-cKO mice. Very recently, Campbell and colleagues also generated *fukutin* cKO mice, using Myf5-Cre and MCK-Cre mice (30). Pathological analysis of our Myf5-fukutin-cKO and MCK-fukutin-cKO mice showed results that were mostly consistent with those reported by Campbell and colleagues: increased serum CK levels in both cKO lines; milder phenotypes of MCK-fukutin-cKO than Myf5-fukutin-cKO; and decreases in grip strength, body mass and longevity of Myf5-fukutin-cKO mice. Our study includes further detailed histopathological characterization of the disease onset and progression in both lines. More importantly, our present study clarifies features of dystroglycanopathy that

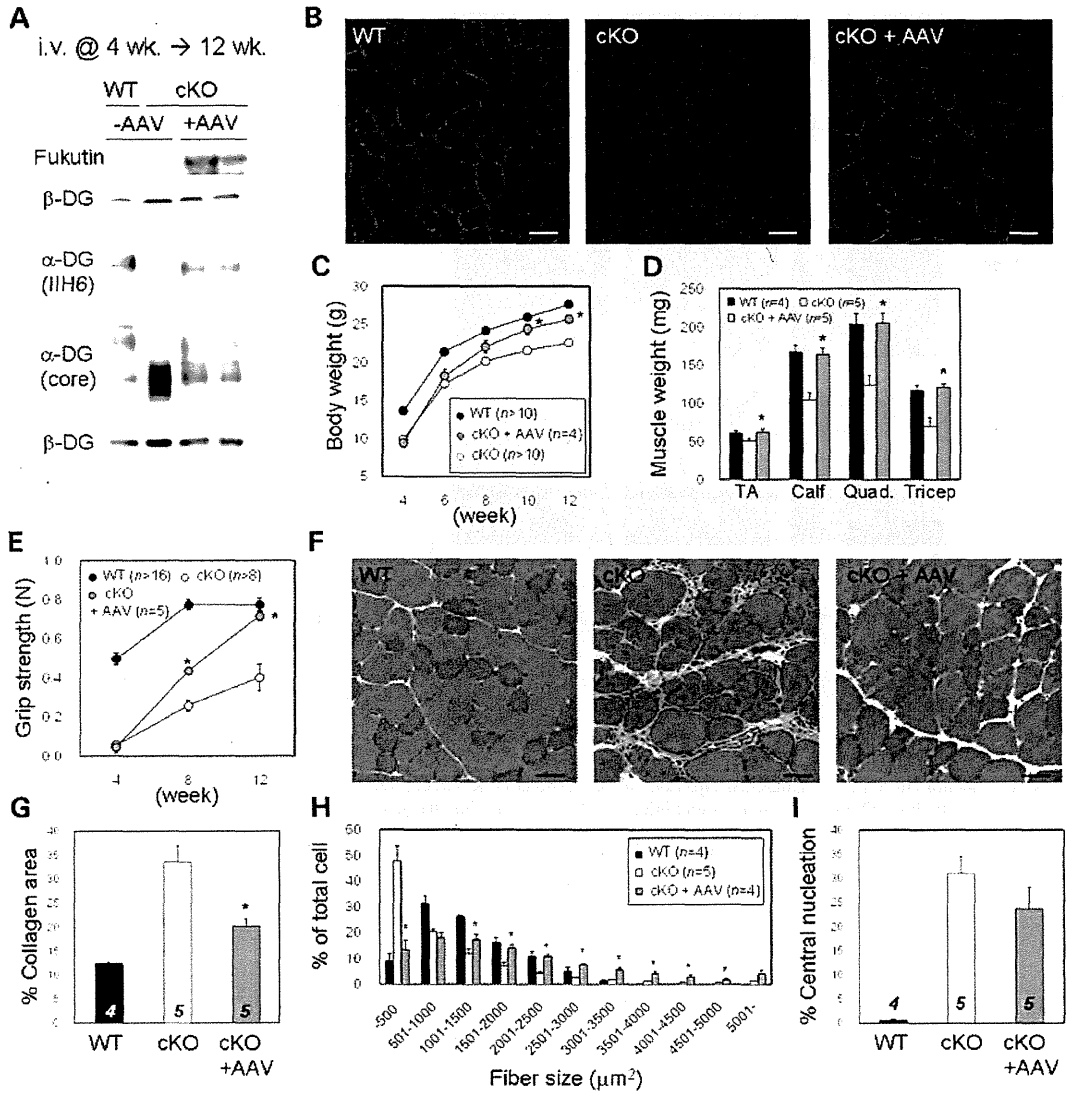

Figure 5. Systemic gene transfer of *fukutin* into Myf5-fukutin-cKO mice. AAV9-MCK-*fukutin* was administered to 4-week-old Myf5-fukutin-cKO mice via tail vein injection. Two months after the gene transfer, the skeletal muscles were analyzed and compared with non-treated Myf5-fukutin-cKO muscles. Recovery of fukutin protein and α-DG modification was confirmed by western blotting (**A**) and immunofluorescence (**B**) (bar □50 μm). For fukutin protein expression and α-DG modification, total lysate and wheat germ agglutinin-enriched fractions, respectively, were subjected to western blotting. In both cases, β-DG was used as a loading control. Therapeutic effects were evaluated by body weight change (**C**; P □0.016 and 0.01 for 10 and 12 weeks, respectively) and muscle weight change (**D**; P □0.047 for tibialis anterior, and 0.014 for other muscles), grip strength (**E**; P □0.007 and 0.003 for 8 and 12 weeks, respectively), H&E staining (**F**) (bar □50 μm), connective tissue infiltration estimated by quantification of collagen I immunoreactive areas (**G**; P □0.028), fiber size variation (**H**; $^*P \leq 0.05$) and central nucleation (**I**). Data from the tibialis anterior muscle are shown (F–I). Histopathology (F) and quantitative analyses (G and H) indicate amelioration of disease severity after the gene transfer. Data shown are mean ± SEM for each group (n is indicated in the graph). $^*P \leq 0.05$ compared with the non-treated cKO mice (Mann–Whitney U test). TA, tibialis anterior; Quad., quadricep.

enhance our understanding of its pathogenesis—specifically, the trigger initiating disease pathogenesis and the biological mechanism underlying the severe phenotype.

Our study provides direct evidence using presymptomatic fukutin-deficient mice that myofiber membrane fragility triggers disease manifestation. Although histological data in both studies suggested regeneration delay or impairment in Myf5-fukutin-cKO skeletal muscles, our study provides the first direct evidence for impaired MPC activity and viability using the isolated myoblast culture system. We observed that the proliferation and differentiation activities of the isolated MPCs from little-affected young Myf5-fukutin-cKO muscles were decreased, which may suggest that fukutin-dependent modification of α-DG plays a role in MPCs. Furthermore, our data showed that MPC proliferation and muscle regeneration deteriorate more severely as the disease progresses. The mechanisms underlying the decreases in the number of isolated satellite cells and MPC proliferation are